J|A|C|S
ARTICLES
Published on Web 10/17/2002

Cyclooctatetraene Computational Photo- and Thermal Chemistry: A Reactivity Model for Conjugated Hydrocarbons

Marco Garavelli,*,† Fernando Bernardi,*,† Alessandro Cembran,† Obis Castaño,‡ Luis Manuel Frutos,‡ Manuela Merchán,§ and Massimo Olivucci*,||

Contribution from the Dipartimento di Chimica "G. Ciamician", Università di Bologna, Via Selmi 2, 40126 Bologna, Italy, Departamento de Química Física, Universidad de Alcalá, 28871 Alcalá de Henares (Madrid), Spain, Departamento de Química Física, Instituto de Ciencia Molecular, Dr. Moliner, 50, 46100 Burjassot, Valencia, Spain, and Istituto di Chimica Organica, Università di Siena, Via Aldo Moro, I-53100 Siena, Italy e Centro per lo Studio dei Sistemi Complessi, Via Tommaso Pendola 37, Siena I-53100 Italy

Received May 24, 2002

Abstract: We use ab initio CASSCF and CASPT2 computations to construct the composite multistate relaxation path relevant to cycloocta-1,3,5,7-tetraene singlet photochemistry. The results show that an efficient population of the dark excited state (S_1) takes place after ultrafast decay from the spectroscopic excited state (S_2). A planar D_{8h}-symmetric minimum represents the collecting point on S_1. Nonadiabatic transitions to S_0 appear to be controlled by two different tetraradical-type conical intersections, which are directly accessible from the S_1 minimum following specific excited-state reaction paths. The higher-energy conical intersection belongs to the same type of intersections previously documented in linear and cyclic conjugated hydrocarbons and features a triangular $-(CH)_3-$ kink. This point mediates both cis → trans photoisomerization and cyclopropanation reactions. The lowest energy conical intersection has a boat-shaped structure. This intersection accounts for production of semibullvalene or for double-bond shifting. The mapping of both photochemical and thermal reaction paths (including also Cope rearrangements, valence isomerizations, ring inversions, and double-bond shifting) has allowed us to draw a comprehensive reactivity scheme for cyclooctatetraene, which rationalizes the experimental observations and documents the complex network of photochemical and thermal reaction path interconnections. The factors controlling the selection and accessibility of a number of conjugated hydrocarbon prototype conical intersections and ground-state relaxation channels are discussed.

1. Introduction

Direct UV-irradiation of cyclooctatetraene (**COT**, **1**) may be of preparative value in the synthesis of semibullvalene (**SBV**, **2**).[1] While in solution this method affords benzene (and acetylene) as an appreciable byproduct,[1] in the vapor phase (∼70 °C) UV irradiation (∼300 nm) has been found to minimize concomitant benzene formation,[2] the method being one of simplicity and essentially quantitative yield (eq a).

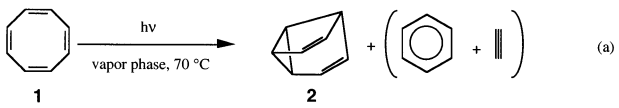

(a)

* To whom correspondence should be addressed. E-mail: (M.G.) mgara@ciam.unibo.it; (M.O.) olivucci@unisi.it; (F.B.) nando@ciam.unibo.it.
† Università di Bologna.
‡ Universidad de Alcalá.
§ Instituto de Ciencia Molecular.
|| Università di Siena.

(1) Zimmerman, H. E.; Iwamura, H. *J. Am. Chem. Soc.* **1970**, *92*, 2015.
(2) Turro, N. J.; Liu, J.-M.; Zimmerman, H. E.; Factor, R. E. *J. Org. Chem.* **1980**, *45*, 3511.

On the basis of experimental observations, Zimmerman et al. presented an extended discussion of the possible mechanistic pathways for the **1** → **2** photoisomerization.[1] Low-temperature irradiation was monitored by low-temperature infrared analysis: evidence was obtained for the direct formation of semibullvalene, or at least against the production of an S_0 intermediate. In particular, both the bicyclic triene bicyclo-[4,2,0]-octa-2,4,7-triene (**BIC**, **3**) and the tricyclic diene tricyclo-[3,3,0,0]-octa-3,7-diene (**4**) were ruled out as possible intermediates,[1] as shown in eqs b and c. A two-photon process for **1** → **2** photoconversion was thus proposed,[1] where the first photon is absorbed by **1** (i.e., the stable *cis*,*cis*,*cis*,*cis* isomer of cyclooctatetraene), leading to production of the strained *trans*,*cis*,*cis*,*cis* isomer (**COT$_{tr}$**, **5**). In a subsequent step, **5** was supposed to absorb a second photon to produce semibullvalene rapidly, because no evidence for accumulation of such an intermediate could be found in the low-temperature experiments (eq d).

Double-bond shifting is another process occurring in anti-aromatic [4*n*] systems such as cyclooctatetraene ($n = 2$). It is well established that the reversible interconversion between double-bond shift isomers (a π-skeletal rearrangement) may be

10.1021/ja020741v CCC: $22.00

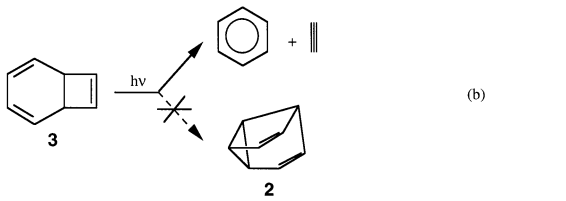

(b)

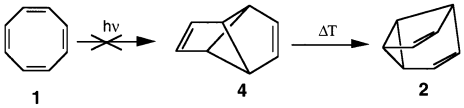

(c)

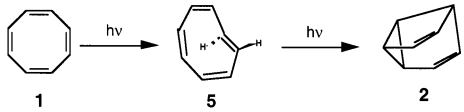

(d)

induced either thermally or photochemically.[3−7] The process occurs when the π-electrons "migrate" within the octagonal perimeter resulting in a site exchange between singly and doubly bonded carbon atoms (**1** → $\mathbf{1_{DBS}}$), as shown in eq e.

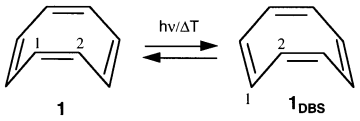

(e)

While double-bond shifting is of no practical interest for parent cyclooctatetraene (yielding the degenerate product $\mathbf{1_{DBS}}$), it may be used to turn on or off conjugation between π-substituents placed in vicinal position (1,2-disubstituted-cyclooctatetraene). Thus, the double-bond shifting reaction may be exploited to design thermally or photochemically driven molecular switches.[7] This principle is described in eq f, where a double-bond shifting is used to interconvert the system between an "on-state", which possesses "through-conjugation" between the π-donor (D) and π-acceptor (A) substituents, and an "off-state", where this through-conjugation is suppressed.

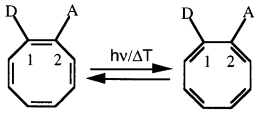

(f)

Thermal double-bond shifting (**1** → $\mathbf{1_{DBS}}$) and ring inversion between the D_{2d}-symmetric equivalent tub forms of cyclooctatetraene (**1** → **1′**) have been investigated both experimentally and computationally.[3−7] NMR and computational studies have shown the barrier for thermal cyclooctatetraene double-bond shifting to be about 14 kcal/mol,[8,9] while the one for ring inversion is only 3−4 kcal/mol lower.[9−11] In this respect, Borden and co-workers[3−5] showed that the thermal double-bond shifting transition state ($\mathbf{TS_{DBS}}$) has a planar D_{8h}-symmetric structure (which violates Hund's rule), while cyclooctatetraene ring inversion proceeds through a planar D_{4h} transition state ($\mathbf{TS_{RI}}$); see eq g.

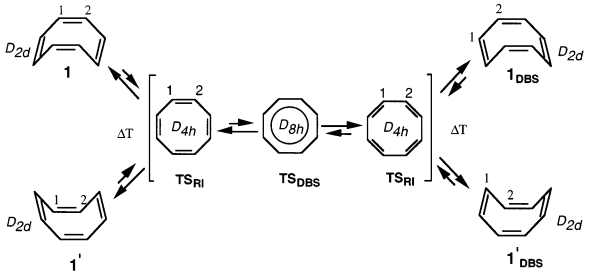

(g)

Cyclooctatetraene is also involved in two thermal valence isomerization reactions (eq h). One (at ∼100 °C) produces the bicyclic isomer **3** with an energy barrier of 28.1 kcal/mol.[12] The other (observed at ∼300 °C)[13] leads to the two semibullvalene isomers **2** and **2′**, with an observed energy barrier of 42.2 ± 0.2 kcal/mol.[14] Semibullvalene appears to have a very low energy barrier (5.5 kcal/mol)[15] for **2** → **2′** Cope rearrangement (eq h). All of these thermal processes (i.e., valence isomerization and Cope rearrangement) have been the subject of extensive and recent high level computational investigations.[16−21]

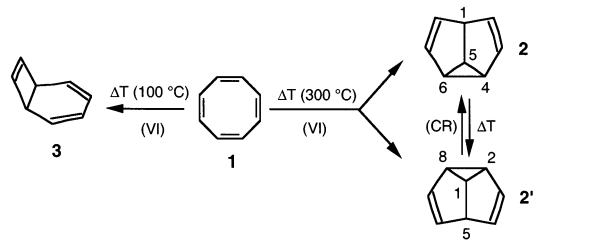

(h)

We have recently shown[22] that photochemical semibullvalene formation and double-bond shifting are two intrinsically competitive processes. In particular, we have provided computational evidence that both photoinduced polycyclization to semibullvalene and double-bond shifting occur via an efficient radiationless decay of photoexcited cyclooctatetraene through the *same* S_1/S_0 conical intersection funnel.

(3) Hrovat, D. A.; Borden, W. T. *J. Am. Chem. Soc.* **1992**, *114*, 5879.
(4) Wenthold, P. G.; Hrovat, D. A.; Borden, W. T.; Lineberger, W. C. *Science* **1996**, *272*, 1456.
(5) Stevenson, C. D.; Brown, E. C.; Hrovat, D. A.; Borden, W. T. *J. Am. Chem. Soc.* **1998**, *120*, 8864.
(6) Paquette, L. A. *Acc. Chem. Res.* **1993**, *26*, 57.
(7) Briquet, A. A. S.; Uebelhart, P.; Hansen, H. J. *Helv. Chim. Acta* **1996**, *79*, 2282.
(8) Anet, F. A. L. *J. Am. Chem. Soc.* **1962**, *84*, 671.
(9) Oth, J. F. M. *Pure Appl. Chem.* **1971**, *25*, 573.
(10) Anet, F. A. L.; Bourn, A. J.; Lin, Y. S. *J. Am. Chem. Soc.* **1964**, *86*, 3576.
(11) Paquette, L. A. *Pure Appl. Chem.* **1982**, *54*, 987.
(12) Huisgen, R.; Mietzsch, F. *Angew. Chem., Int. Ed. Engl.* **1964**, *3*, 83.
(13) Martin, H.-D.; Urbanek, T.; Walsh, R. *J. Am. Chem. Soc.* **1985**, *107*, 5532.
(14) Hassenruck, K.; Martin, H.-D.; Walsh, R. *Chem. Rev.* **1989**, *89*, 1125 and references therein.
(15) (a) Cheng, A. K.; Anet, F. A. L.; Mioduski, J.; Meinwald, J. *J. Am. Chem. Soc.* **1974**, *96*, 2887. (b) Moskau, D.; Aydin, R.; Leber, W.; Gunther, H.; Quast, H.; Martin, H.-D.; Hassenruck, K.; Miller, L. S.; Grohmann, K. *Chem. Ber.* **1989**, *122*, 925.
(16) Castano, O.; Frutos, L.-M.; Palmeiro, R.; Notario, R.; Andres, J.-L.; Gomperts, R.; Blancafort, L.; Robb, M. A. *Angew. Chem., Int. Ed.* **2000**, *39*, 2095.
(17) Castano, O.; Notario, R.; Gomperts, R.; Abboud, J.-L. M.; Palmeiro, R.; Andres, J.-L. *J. Phys. Chem. A* **1998**, *102*, 4949.
(18) Andres, J.-L.; Castano, O.; Morreale, A.; Palmeiro, R.; Gomperts, R. *J. Chem. Phys.* **1998**, *108*, 203.
(19) (a) Palmeiro, R.; Frutos, L.-M.; Castano, O. *Int. J. Quantum Chem.* **2002**, *86*, 422. (b) Castano, O.; Palmeiro, R.; Frutos, L.-M.; Andres, J.-L. *J. Comput. Chem.* **2002**, *23*, 732.
(20) Jiao, H. J.; Schleyer, P. V. *Angew. Chem., Int. Ed. Engl.* **1993**, *32*, 1760.
(21) Jiao, H. J.; Nagelkerke, R.; Kurtz, H. A.; Williams, R. V.; Borden, W. T.; Schleyer, P. V. *J. Am. Chem. Soc.* **1997**, *119*, 5921.
(22) Garavelli, M.; Bernardi, F.; Moliner, V.; Olivucci, M. *Angew. Chem., Int. Ed.* **2001**, *40*, 1466.

In the present paper, we significantly extend the investigation of photochemically relevant potential energy surfaces of cyclooctatetraene. The results support immediate radiationless decay of the bright (S_2) state into the dark lowest excited state (S_1). Subsequent relaxation along the S_1 path prompts population of an excited (S_1) planar minimum with D_{8h} symmetry (**COT***, **6**). This is the collecting point for photoexcited molecules. Ground-state decay of **6** is prompted by evolution along two barrier-controlled S_1/S_0 conical intersections. One conical intersection is similar to that documented for other unsaturated hydrocarbons[23−29] and displays a typical out-of-plane triangular $-(CH)_3-$ kink of triradical nature. The second conical intersection corresponds to the one recently reported in a previous study.[22] To draw a full comprehensive reactivity scheme comprising all of the thermal and photochemical reactions (and their interconnections), we have studied the following aspects: (i) the structure of the singlet manifold (S_0, S_1, S_2, S_3) in the Franck−Condon (FC) region of cyclooctatetraene, (ii) the initial relaxation path (prompting population of **COT***) leading from the spectroscopic state S_2 to the dark state S_1, (iii) the alternative routes for the S_1 evolution and $S_1 \rightarrow S_0$ decay of **COT***, and (iv) the thermal reaction paths connecting cyclooctatetraene and its photoproducts along the S_0 energy surface (reinvestigating also previously studied processes such as valence isomerization, Cope rearrangement, ring inversion, and double-bond shift).

In the discussion section, the data i−iv will be used to determine the substituent, steric, and electronic factors, playing a role in cyclooctatetraene photochemistry and associated photoproducts selection. The conical intersection structures responsible for the photochemistry of *cyclic conjugated hydrocarbons* (i.e., photoproducts formation and distribution) will be discussed, and a qualitative-predictive model will be proposed with cyclooctatetraene taken as a paradigm. Speculations about applicability and limits of cyclooctatetraene double-bond shift-based molecular switches will be finally considered.

2. Computational Methods

All CASSCF minimum energy path (MEP) computations on S_1 and S_0 have been carried out using the split-valence + polarization 6-31G* basis set. The active space in our computations is unambiguously defined: it comprises all of the π electrons and valence π-orbitals of the polyene. Thus, a full active space of eight electrons in eight π-orbitals has always been used for potential energy surface mapping, such as critical points and conical intersections optimizations, analytical frequency calculations, and minimum energy path computations, using the Gaussian 98 suite of quantum-chemical programs.[30]

IRD computations have been used for locating all of the possible S_0 relaxation channels departing from the lower tip of a conical intersection point.[31,32] This is accomplished first via locating an initial direction of relaxation (IRD) on S_0 (as close as possible to the conical intersection),[31,32] and second via standard minimum energy path computations following that IRD. Briefly, an IRD corresponds to a local *steepest descent direction*, in *mass-weighted Cartesians*, from a given starting point. The IRD is calculated by locating the energy minimum on a hyperspherical (i.e., *n*-1-dimensional) cross section of the *n* dimensional potential energy surface (*n* is the number of vibrational degrees of freedom of the molecule) centered on the starting point (the S_1/S_0 conical intersection in this case). The radius of this hypersphere is usually chosen to be small (typically 0.25−0.5 au in *mass-weighted Cartesians*) to locate the steepest direction in the vicinity of the starting point (i.e., the hypersphere center). The IRD is then defined as the vector joining the starting point to the energy minimum (a *hyperminimum*). Once one or more *hyperminima* have been determined, the associated minimum energy path (emerging from these points) is computed as *the steepest descent line in mass-weighted Cartesians*[33] using the IRD vector to define the initial direction to follow.

These relaxation channels describe the *static* (i.e., *nondynamical*) evolution of the system after decay to the ground state and provide insight into the mechanism of photoproduct formation in conditions of vibrationally "cold" molecules (i.e., with infinitesimal velocity). Although molecules have more than infinitesimal kinetic energy (and in fact classical trajectories deviate from this static paths), nevertheless minimum energy paths may represent a convenient measure of the progress of a molecule in a photochemical reaction, provided that it occurs in a cold environment where slow excited-state motion or/and thermal equilibration is possible and the excited-state reactant has a small/controlled amount of vibrationally excess energy. Under these conditions, semiclassical dynamics yield the same mechanistic information as from topological investigation of the potential energy surface, because its structure is expected to play the dominant role in determining the initial molecular motion in the decay region. This strategy has been successfully applied in previous computational investigations involving conjugated hydrocarbons photochemistry[23−27,32] and has been validated by semiclassical dynamics computations.[32,34,35] Thus, we are confident this approach may help to understand and rationalize the photochemical behavior of cyclooctatetraene.

To improve the computed energetics, the effect of dynamic electron correlation has also been included. The S_1 and S_0 energies along the fully optimized minimum energy paths have been recomputed by using multiconfigurational second-order perturbation theory via the CASPT2 approach[36] included in the MOLCAS-5 package.[37] A reference CASSCF/6-31G* wave function with the standard (eight electrons in eight π-orbitals) active space has always been used for all CASPT2 (PT2 hereafter) computations. In addition, CASSCF/6-31G* zero-point energy (ZPE) corrections have been included when stated.

It is worth noting how PT2 corrections shift the position of the CASSCF optimized S_1/S_0 conical intersection points toward the relaxed

(23) Celani, P.; Garavelli, M.; Ottani, S.; Bernardi, F.; Robb, M. A.; Olivucci, M. *J. Am. Chem. Soc.* **1995**, *117*, 11584.
(24) Garavelli, M.; Celani, P.; Yamamoto, N.; Bernardi, F.; Robb, M. A.; Olivucci, M. *J. Am. Chem. Soc.* **1996**, *118*, 11656.
(25) Garavelli, M.; Celani, P.; Bernardi, F.; Robb, M. A.; Olivucci, M. *J. Am. Chem. Soc.* **1997**, *119*, 11487.
(26) Palmer, I. J.; Ragazos, I. N.; Bernardi, F.; Olivucci, M.; Robb, M. A. *J. Am. Chem. Soc.* **1993**, *115*, 673.
(27) Garavelli, M.; Frabboni, B.; Fato, M.; Celani, P.; Bernardi, F.; Robb, M. A.; Olivucci, M. *J. Am. Chem. Soc.* **1999**, *121*, 1537.
(28) Robb, M. A.; Garavelli, M.; Olivucci, M.; Bernardi, F. *Reviews in Computational Chemistry*; 2000; Vol. 15, pp 87−146.
(29) Bernardi, F.; Olivucci, M.; Robb, M. A. *Chem. Soc. Rev.* **1996**, *25*, 321.
(30) Frisch, M. J.; Trucks, G. W.; Schlegel, H. B.; Scuseria, G. E.; Robb, M. A.; Cheeseman, J. R.; Zakrzewski, V. G.; Montgomery, J. A., Jr.; Stratmann, R. E.; Burant, J. C.; Dapprich, S.; Millam, J. M.; Daniels, A. D.; Kudin, K. N.; Strain, M. C.; Farkas, O.; Tomasi, J.; Barone, V.; Cossi, M.; Cammi, R.; Menucci, B.; Pomelli, C.; Adamo, C.; Clifford, S.; Ochterski, J.; Petersson, G. A.; Ayala, P. Y.; Cui, Q.; Morokuma, K.; Malick, D. K.; Rabuck, A. D.; Raghavachari, K.; Foresman, J. B.; Cioslowski, J.; Ortiz, J. V.; Stefanov, B. B.; Liu, G.; Liashenko, A.; Piskorz, P.; Komaromi, I.; Gomperts, R.; Martin, R. L.; Fox, D. J.; Keith, T.; Al-Laham, M. A.; Peng, C. Y.; Nanayakkara, A.; Gonzalez, C.; Challacombe, M.; Gill, P. M. W.; Johnson, B. G.; Chen, W.; Wong, M. W.; Andres, J.-L.; Gonzalez, C.; Head-Gordon, M.; Replogle, E. S.; Pople, J. A. *Gaussian 98*, revision A.6; Gaussian, Inc.: Pittsburgh, PA, 1998.
(31) Celani, P.; Robb, M. A.; Garavelli, M.; Bernardi, F.; Olivucci, M. *Chem. Phys. Lett.* **1995**, *243*, 1.
(32) Garavelli, M.; Celani, P.; Fato, M.; Bearpark, M. J.; Smith, B. R.; Olivucci, M.; Robb, M. A. *J. Phys. Chem. A* **1997**, *101*, 2023.
(33) Gonzalez, C.; Schlegel, H. B. *J. Phys. Chem.* **1990**, *94*, 5523.
(34) Garavelli, M.; Bernardi, F.; Olivucci, M.; Bearpark, M. J.; Klein, S.; Robb, M. A. *J. Phys. Chem. A* **2001**, *105*, 11496.
(35) Vreven, T.; Bernardi, F.; Garavelli, M.; Olivucci, M.; Robb, M. A.; Schlegel, H. B. *J. Am. Chem. Soc.* **1997**, *119*, 12687.
(36) Andersson, K.; Malmqvist, P.-Å.; Roos, B. O. *J. Chem. Phys.* **1992**, *96*, 1218.
(37) Andersson, K.; Blomberg, M. R. A.; Fülscher, M. P.; Karlström, G.; Lindh, R.; Malmqvist, P.-Å.; Neogrády, P.; Olsen, J.; Roos, B. O.; Sadlej, A. J.; Schütz, M.; Seijo, L.; Serrano-Andrés, L.; Siegbahn, P. E. M.; Widmark, P.-O. Molcas 5.0; Lund University: Lund, 1999.

Scheme 1

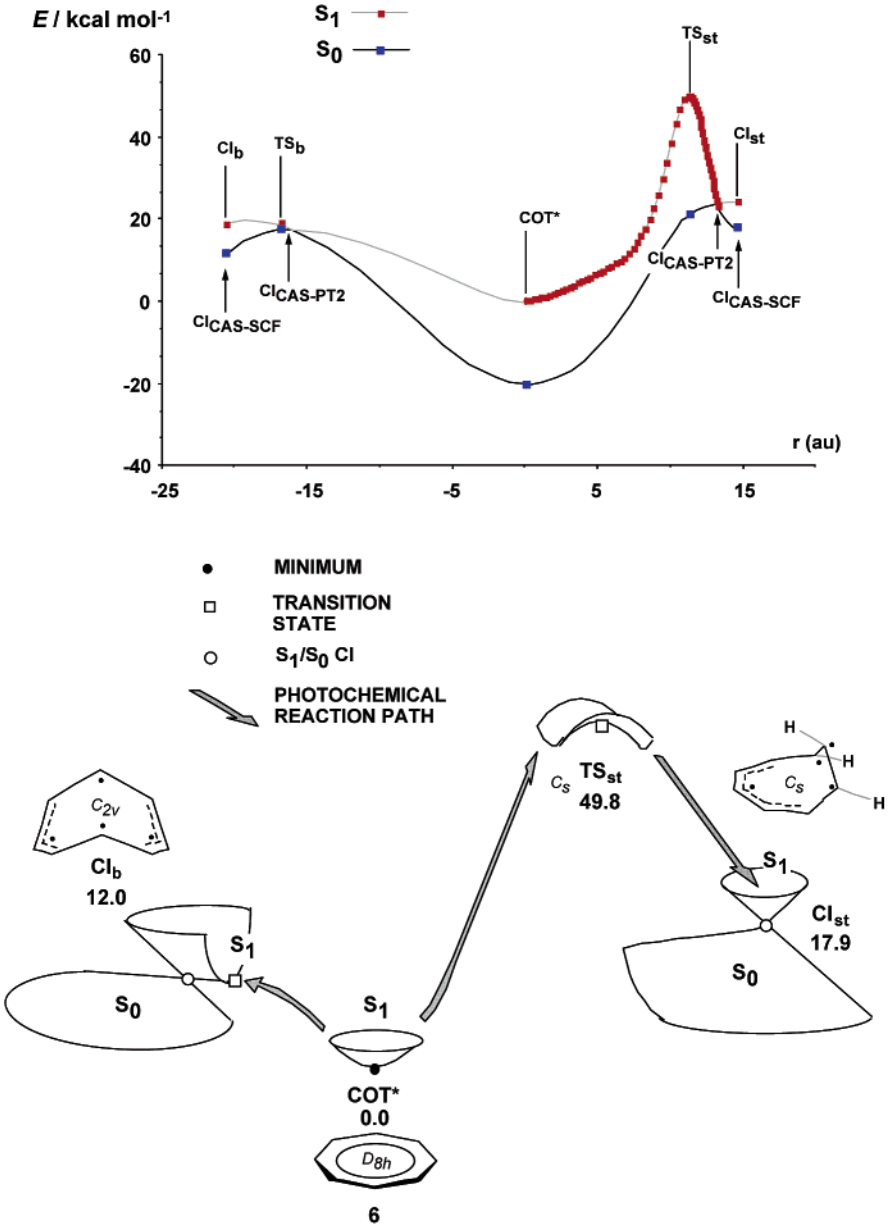

S_1-excited cyclooctatetraene structure (**6**; see Scheme 1). Anyway, to evaluate the effect of dynamic electron correlation on the geometry optimization is not trivial,[38] and because all surface mapping has been performed using CASSCF, the CASSCF optimized S_1/S_0 conical intersections have been taken as starting points for S_0 relaxation paths mapping.

The energies for the singlet manifold (S_0, S_1, S_2, S_3) reported in Table 1 and Figure 1 have been computed with the PT2 method and have been used, together with the RASSI approach,[39] to compute the oscillator strengths (*f*) for vertical electronic transitions (see Table 1).[39] Again, a reference CASSCF wave function has been used with a 6-31G* basis set and the standard (eight electrons in eight π-orbitals) active space. State-average CASSCF computations have been performed between states with the same symmetry, which have been averaged with identical weights. These results have also been validated and reproduced using a generally contracted basis set of atomic natural orbitals (ANO-L) obtained from the C(14s9p4d)/H(8s4p) primitive sets with the C[4s3p2d]/H[2s1p] contraction scheme[40,41] (results not shown). In perturbation theories (like CASPT2), a very common problem is the appearance of intruder states. For a given excited state, it is usually reflected in the relatively low weight (ω), with respect to that obtained for the ground state, of the corresponding CASSCF reference in the first-order wave function. In those cases, a number of calibration calculations have been carried out using a level-shift technique, and the influence of weakly interacting intruder states on the computed excitation energies has been checked. In particular, the so-called imaginary level shift[42] implemented in the MOLCAS-5 suite of programs[37] has been employed, because it is capable of removing singularities completely. For this purpose, excitation energies have been computed with different values of the level shift parameter (IMAG): 0.0 (standard CASPT2 theory), 0.1, 0.2, 0.3, and 0.4 au. It is found

(38) Olivucci, M.; Page, C. S., in preparation.
(39) Malmqvist, P.-Å.; Roos, B. O. *Chem. Phys. Lett.* **1989**, *155*, 189. RASSI has been used to compute the transition dipole moments from the CASSCF reference wave functions. The oscillator strength (*f*) is defined as $f = {}^2/_3|M_{if}|^2\Delta E_{fi}$, where M_{if} is the transition dipole moment (in au), and ΔE_{fi} is the CASPT2 excitation energy (in au).
(40) Widmark, P.-O.; Malmqvist, P.-Å.; Roos, B. O. *Theor. Chim. Acta* **1990**, *77*, 291.
(41) Widmark, P.-O.; Persson, B. J.; Roos, B. O. *Theor. Chim. Acta* **1991**, *79*, 419.
(42) Forsberg, N.; Malmqvist, P.-Å. *Chem. Phys. Lett.* **1997**, *274*, 196.

Table 1. Total (E) and Relative (ΔE) CASSCF and CASPT2 (6-31G*) Energies of the Singlet Manifold (S_0, S_1, S_2, and S_3) for Cyclooctatetraene Relaxation out of the FC Region (See Discussion in the Text and Also the Energy Profiles in Figure 1): Values in au (Hartree) and kcal mol^{-1}, Respectively[a]

		E + 307 au[b]		ΔE (kcal mol^{-1})		f [c]
structures[d]	state[e]	CASSCF	CASPT2 (ω)	CASSCF	CASPT2	CASPT2
COT (D_{2d})	$S_0(1^1A_1)$	−0.618368	−1.537640(0.76)	0.0	0.0	
(**1**)	$S_1(1^1A_2)$	−0.388459	−1.390580(0.73)	144.3	92.3	forbidden
	S_2 (1^1E)	−0.360835	−1.326304(0.75)	161.6	132.6	0.0068
	$S_3(2^1A_1)$	−0.378099	−1.317077(0.63)[f]	150.8	138.4	forbidden
TS$_{RI}$ (D_{4h})	$S_0(1^1A_{1g})$	−0.612008	−1.524331(0.76)	4.0	8.4	
	$S_1(1^1A_{2g})$	−0.469375	−1.451949(0.74)	93.5	53.8	forbidden
	$S_2(2^1A_{1g})$	−0.506827	−1.435574(0.76)	70.0	64.0	forbidden
	$S_3(1^1E_u)$	−0.401875	−1.347476(0.48)[f]	135.8	119.3	0.0051
S_2/S_1 **CI$_{opt}$** (D_{2d})	$S_0(1^1A_{1g})$	−0.609744	−1.523380(0.76)	5.4	8.9	
	$S_1(1^1A_{2g})$	−0.486312	−1.467654(0.76)	82.9	43.9	forbidden
	$S_2(2^1A_{1g})$	−0.541434	−1.471382(0.74)	48.3	41.6	forbidden
	$S_3(1^1E_u)$	−0.418990	−1.362325(0.73)	125.1	110.0	0.0056
COT* (D_{8h})	$S_0(1^1B_{2g})$	−0.606038	−1.521029(0.75)	7.7	10.4	
(**6**)	$S_1(1^1A_{1g})$	−0.555983	−1.489691(0.73)	39.2	30.1	forbidden
	$S_2(1^1B_{1g})$	−0.492204	−1.472948(0.71)	79.2	40.6	forbidden
	$S_3(1^1E_{1u})$	−0.424390	−1. 367131(0.51)[f]	121.7	107.0	forbidden

[a] The weight (ω) of the CASSCF reference wavefunction (i.e., the zeroth-order function) in the first-order (CASPT2) function is given within parentheses. Values for the oscillator strength (f) are also included. [b] State-average CASSCF calculations have been performed between states of the same symmetry. [c] See ref 39. [d] As defined in the text (see also Figure 1). [e] Ordering of states from the CASPT2 results. [f] Despite the relatively low weight, the excitation energy is stable with respect to the variation of the imaginary level shift parameter[42] (see section 2 for further details).

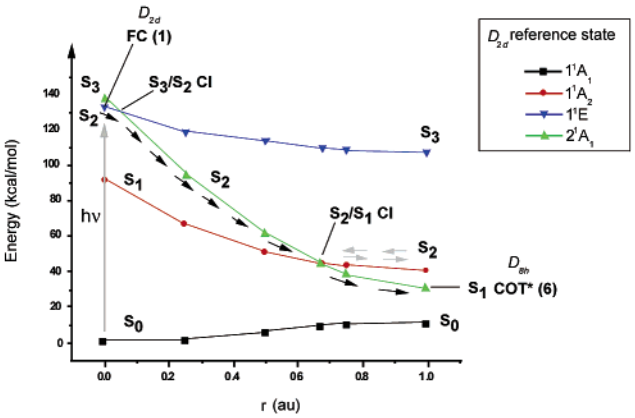

Figure 1. Nonrelaxed linear scan from **1** (FC) to **6** (**COT***) following the D_{2d}-symmetric force vector computed on the FC spectroscopic state S_2. Symmetry labels refer to the D_{2d} symmetry. Distances (r) are expressed in *mass-weighted* atomic units (au): amu$^{1/2}$ bohr.

that the computed excitation energies are invariant within 0.05 eV with respect to the IMAG parameter. Therefore, even if the ω value at IMAG = 0.0 au is somewhat low in certain cases for the highest excited state here considered (S_3 state), the computed excitation energy can confidently be trusted. All of these calculations were carried out with the tools available in the MOLCAS-5 package.[37]

All of the computed energies are reported and summarized in Tables 1 and 2. A nonrelaxed linear scan from the D_{2d} FC structure (**1**) to the D_{8h} excited (S_1) minimum (**6**) is reported in Figure 1 and has been performed in mass-weighted internal coordinates. The direction of this rigid scan appears to be parallel to the direction of the initial D_{2d}-symmetric force vector computed at the FC point of the lowest dipole-allowed state (S_2). Therefore, the reported scan follows the natural relaxation direction out of the FC region (i.e., the force direction) and preserves the D_{2d} symmetry all along the path (see section 3.1).

3. Computational Results

3.1. Spectroscopy and Relaxation from the FC Region: The $S_2 \rightarrow S_1$ Deactivation Path. The electronic ground state (S_0) for the D_{2d} tube form (**1**) of cyclooctatetraene (i.e., the starting reactant and ground-state minimum) has a $^1A_1$ symmetry. Electronic transitions from S_0 to the excited S_1 and S_3 states (possessing a $^1A_2$ and $^1A_1$ symmetry, respectively) are forbidden (see Table 1). In fact, for a dipole-allowed electronic transition, the product A × B × C (where A, C, and B represent the irreducible representation of the wave function in the initial state, the final state, and the component (x,y,z) of the dipole moment, respectively) has to belong to the totally symmetric representation. Because the products $A_1 \times B_2 \times A_2$ or $A_1 \times E \times A_2$ do not span the totally symmetric representation (A_1 for D_{2d} symmetry group), the $S_0 \rightarrow S_1$ electronic transition, related mainly to the HOMO → LUMO singly excited configuration, is forbidden. The same occurs for the $S_0 \rightarrow S_3$ transition, involving the (HOMO → LUMO)^2 two-electron promotion. On the other hand, transition to the electronic state S_2 (a double degenerate state owning a ^{1}E symmetry and described mainly by two coupled singly excited configurations: HOMO, HOMO−1 → LUMO,LUMO+1) is dipole-allowed (the oscillator strength for this transition being $\sim 7 \times 10^{-3}$). Hence, the $S_0(^1A_1) \rightarrow S_2(^1E)$ electronic transition can be assigned as the lowest dipole-allowed absorption feature and, accordingly, the FC S_2 state has been taken as the starting point for the excited-state relaxation of the system.

The optical absorption spectrum and electron-impact energy-loss spectrum of cyclooctatetraene can be described as a broad maximum of low intensity over the region 310−260 nm (4.00−4.77 eV) and a strong feature with an intensity maximum at 6.42 eV.[43a] As can be seen in Table 1, the computed vertical excitation energies for **1** are predicted with an exceedingly weak intensity. As stated above, two of them are actually dipole-

(43) (a) Frueholz, R. P.; Kuppermann, A. *J. Chem. Phys.* **1978**, *69*, 3614. (b) Traetteberg, M. *Acta Chem. Scand.* **1966**, 1724. (c) Palmer, M. H. *J. Mol. Struct.* **1988**, *178*, 79. (d) Van-Catledge, F. A. *J. Am. Chem. Soc.* **1971**, *93*, 4365. (e) Roos, B. O.; Merchán, M.; McDiarmid, R.; Xing, X. *J. Am. Chem. Soc.* **1994**, *116*, 5927. (f) Serrano-Andrés, L.; Lindh, R.; Roos, B. O.; Merchán, M. *J. Phys. Chem.* **1993**, *97*, 9360. (g) The *diabatic* components of the *adiabatic* electronic eigenfunctions describe the energy of a particular spin-coupling, while the *adiabatic* functions represent the surfaces of the real states (the singlet ground and excited states, in this case): Olivucci, M. *Superfici Adiabatiche e Diabatiche nel Trattamento della Reattività Chimica*, Ph.D. Thesis, Dipartimento di Chimica 'G. Ciamician'; Universita' di Bologna: Bologna, 1988.

Table 2. Total (*E*) and Relative (ΔE) CASSCF and CASPT2 (6-31G*) Energies for All of the S_1 and S_0 Structures Discussed in the Text: Values in au (Hartree) and kcal mol^{-1}, Respectively[a]

		E + 307 au[b]		ΔE (kcal mol^{-1})		ZPE[b]
structures[c]	state[d]	CASSCF	CASPT2 (ω)	CASSCF	CASPT2	CASSCF
COT* (6)[e]	S_1	−0.55714	−1.48067 (0.76)	0.0	0.0	90.2
TS_{DBS} (6)[e]	S_0	0.60904	−1.51274 (0.76)	−32.6	−20.1	85.2
TS_b	S_1[f]	−0.51403[g]	−1.45236 (0.75)[g]	27.1	18.0	
	S_1[f]	−0.51662[h]		25.4		87.4
	S_0[f]	−0.53032[g]	−1.45058 (0.76)[g]	16.8	19.2	
TS_{st}	S_1	−0.47953	−1.40131 (0.73)	48.7	49.8	84.4
	S_0	−0.53026	−1.44727 (0.75)	16.9	21.0	
CI_b	S_1[f]	−0.51695[g]	−1.46159 (0.75)[g]	25.2	12.0	
	S_0[f]	−0.52427[g]	−1.44985 (0.75)[g]	20.6	19.3	
	S_0[f]	−0.52915[h]	−1.44961 (0.76)[h]	17.6	19.5	
CI_{st}	S_1[f]	−0.51102[g]	−1.45208 (0.75)[g]	28.9	17.9	
	S_0[f]	−0.51457[g]	−1.44156 (0.75)[g]	26.7	24.5	
	S_0[f]	−0.51930[h]	−1.44069 (0.76)[h]	23.7	25.1	
COT (1)	S_0	0.63567	−1.53381 (0.77)	−49.2	−33.3	87.4
DIR	S_0	0.58801	−1.52402	−19.4	−27.2	86.9
TS_{CR}	S_0	0.58754	−1.52500 (0.75)	−19.1	−27.8	87.0
SBV (2)	S_0	0.60384	−1.53861 (0.76)	−29.3	−36.4	89.2
DIR′ (7)	S_0	0.53394	−1.46296 (0.75)	14.6	11.1	
COT_{tr} (5)	S_0	0.59518	−1.50068 (0.76)	−23.9	−12.6	
$TS_{DIR'}$	S_0	0.52714	−1.46042 (0.75)	18.8	12.7	
TS′	S_0	0.51607	−1.43954 (0.76)	25.8	25.8	
DIR″	S_0	0.51870	−1.43649 (0.76)	24.1	27.7	
TS_{SBV}	S_0	0.50895	−1.43376 (0.76)	30.3	29.4	
$TS1_{VI}$	S_0	0.56892	−1.48922 (0.76)	−7.4	−5.4	86.3
$TS2_{VI}$	S_0	0.54163	−1.47279 (0.75)	9.7	4.9	85.5
BIC (3)	S_0	0.61099	−1.52346 (0.76)	−33.8	−26.9	
TS_{RI}	S_0	0.61915	−1.51397 (0.77)	−38.9	−20.9	87.9

[a] When computed, CASSCF/6-31G* zero-point energies (ZPE) are also reported (in kcal mol^{-1}). The weight (ω) of the CASSCF reference wavefunction (i.e., the zeroth-order function) in the first-order (CASPT2) function is given within parentheses. [b] Single-state energy computations (unless differently stated). [c] As defined in the text (see also Scheme 11). [d] S_0 and S_1 as from CASSCF energy computations; this corresponds (unless differently stated) to the order established by CASPT2 computations. [e] **COT*** and **TS_{DBS}** correspond to structure **6**. [f] CASSCF and CASPT2 energy order (S_0 and S_1) are inverted. [g] State-average computations between the lowest two singlet states (S_0 and S_1) with weights of 0.5 each. [h] When state averaging is used, a single-state computation is also performed for comparison.

forbidden. Therefore, comparison of the current results with the experimental data has to be limited to the low-energy region of the spectrum (≤6.0 eV).

The lowest singlet excited-state S_1 is of A_2 symmetry in agreement with previous theoretical results [see, e.g., ref 43a,c,d]. That the lowest singlet → singlet transition is optically forbidden was clearly established by Frueholz and Kuppermann in 1978.[43a] The computed vertical excitation energy (4.00 eV, CASPT2 result in Table 1) is somewhat too low as compared to the maximum of the low-intensity band (4.4 eV). It is worth recalling that there is a crucial factor for deviation between computed and recorded transition energies that affects both computed and measured data: the equilibrium geometry for the excited state differs substantially (see below) from that of the ground state. The resulting broad Franck−Condon envelope introduces relatively large uncertainties into experimental band maximum determinations. In addition, because of the steep curvature of the excited-state potential energy surface at the ground-state equilibrium geometry (see Figure 1), small errors in the geometry used for the ground state may lead to a significant error in the computed vertical transition energy. Nevertheless, the computed ground-state geometry is very close to the experimental data derived from electron diffraction.[43b] Therefore, in the case that a higher accuracy would be required (to fully describe on theoretical grounds the observed low-intensity/low-energy band), vibronic interactions have to be taken into account. The band maximum and the vertical transition seem to differ around half an eV, consistent with the expected long Franck−Condon progression. A full theoretical description of the electronic spectrum of cyclooctatetraene is well beyond the scope of this work and is certainly a challenging task: the implied theoretical difficulties are more closely related to a strained, nonplanar diene like norbornadiene (bicyclo-[2.2.1]-hepta-2,5-diene)[43e] than to even polyenes.[43f] However, work in progress considering also valence σ/π, π/σ states and the lowest Rydberg transitions enables us to confirm that the strongest recorded feature in the electronic spectrum of cyclooctatetraene can be related to a higher ^1E state (not documented here), as it was already suggested from pioneering INDO calculations.[43d]

Analysis of the gradient at the FC point reveals that it is very similar for all of the studied states and possesses a D_{2d} symmetry. Full relaxation upon these states leads to similar planar minima, owning the same D_{8h} symmetry. Furthermore, the topology of S_1, S_2, and S_3 around the FC region is similar. From the D_{2d} reactant **1** to the D_{8h} excited (S_1) minimum **6**, a

linear nonrelaxed scan of the potential energy surface for the singlet states (S_0, S_1, S_2, and S_3) has been computed. It was inspired analyzing the initial D_{2d}-symmetric force vector calculated at the FC point of the lowest dipole-allowed state S_2 (see Computational Methods). The corresponding PT2 energy profiles have been reported in Figure 1. The results show that along this D_{2d}-symmetric relaxation coordinate, a sudden crossing between the S_2 and S_3 states takes place (S_3/S_2 **CI** in Figure 1). Therefore, the S_2 potential energy surface rapidly changes its symmetry (from ^1E to $^1A_1$) and electronic nature (from HOMO,HOMO$-1 \rightarrow$ LUMO, LUMO$+1$ to (HOMO $\rightarrow$ LUMO)^2) as a result of a crossing with the steeper S_3 ($^1A_1$) surface occurring along the initial ultrafast dynamics out of the S_2 (^1E) FC region. Following relaxation along the S_2 ($^1A_1$) potential energy surface, the system is driven into a second crossing with the singlet S_1 ($^1A_2$) state. This crossing (S_2/S_1 **CI**) funnels S_2 radiationless decay and prompts S_1 population. Because the final S_1 point **6** is diabatically connected (via S_2/S_1 **CI**) with S_2,[43g] it preserves both the electronic and the symmetric ($^1A_1$) character of S_2.

It is worth noting that, due to the sloped topology[28,44,45] of the conical intersection S_2/S_1 **CI** (see Figure 1), it is also possible to populate the relaxed D_{8h}-symmetric minimum on the S_2 ($^1A_2$) state as a result of the initial dynamics through this crossing.[44] Still, the energy gap separation between S_2/S_1 **CI** (or the optimized $-$ S_2/S_1 $\mathbf{CI_{opt}}$ $-$ conical intersection point) and the relaxed S_2 minimum is very small ($\leq$4 kcal/mol; see Table 1 and Figure 1). Therefore, due to excess vibrational energy following relaxation from the FC region, an appreciable population of the S_2 state should not be expected because an efficient decay to S_1 may be easily prompted overcoming the small activation barrier toward S_2/S_1 **CI**.

In conclusion, after the lowest $S_0(^1A_1) \rightarrow S_2(^1E)$ dipole-allowed transition, the photoexcited system quickly reaches the S_1 state and populates the relaxed D_{8h} excited (S_1) minimum **6**, while a D_{2d} symmetry preserving planarization motion may be involved. Further validation for the computed relaxation comes from the gradient difference and derivative coupling vectors computed at the conical intersection point S_2/S_1 **CI** (see Figure 2) and defining the branching space (i.e., the space which must contain all of the initial paths out of the crossing region).[29] This analysis reveals that any relaxation path starting from this conical intersection must have two initial components: the first one leads to the flattening of the system (Figure 2a), while the second one involves only a π bond-length reorganization leading to double bonds stretching and concomitant single bonds compressing (Figure 2b). Therefore, we have found that the tendency of the system (following decay from S_2/S_1 **CI**) is for a full π-bonds delocalization leading to a flattening of the molecule. This motion is exactly the one which drives the system toward **COT***, that is, the planar D_{8h} structure **6** on S_1 (see Figure 3a). Hence, we conclude that the most likely and favored relaxation path from the S_2 FC point is that leading to the D_{8h} S_1 minimum **6**.[46]

3.2. The S_1 Reaction Paths. In the previous section, we have provided evidence that photoexcited cyclooctatetraene relaxes toward the planar D_{8h}-symmetric minimum **6** residing on the dark (HOMO $\rightarrow$ LUMO)^2 doubly excited-state S_1. Its structure (see Figure 3a) appears to be identical to the thermal double-bond shift transition state ($\mathbf{TS_{DBS}}$) already reported by Borden et al. computationally,[3−5] and also reinvestigated here (see section 3.4). This is the typical π-delocalized structure expected to characterize the relaxed S_1 state for a Hückel antiaromatic [4*n*] system.[3−5]

As the S_1/S_0 energy gap is still quite large here ($\sim$20 kcal/mol), we have looked for deformations along accessible reaction channels leading to real crossing points. Two very different S_1/S_0 conical intersections ($\mathbf{CI_{st}}$ and $\mathbf{CI_b}$) have been located on S_1 (see Scheme 1). Both have a "quasi-tetraradical" electronic nature, but differ clearly in energy, geometry, and symmetry. $\mathbf{CI_{st}}$ (see Figure 3b), which is higher in energy (about 18 kcal/mol above **6**; see Table 2), has a C_s-symmetric structure and appears to be of the same type as the previously documented crossing points involved in the photochemistry of linear and cyclic conjugated hydrocarbons.[23−27] This type of conical

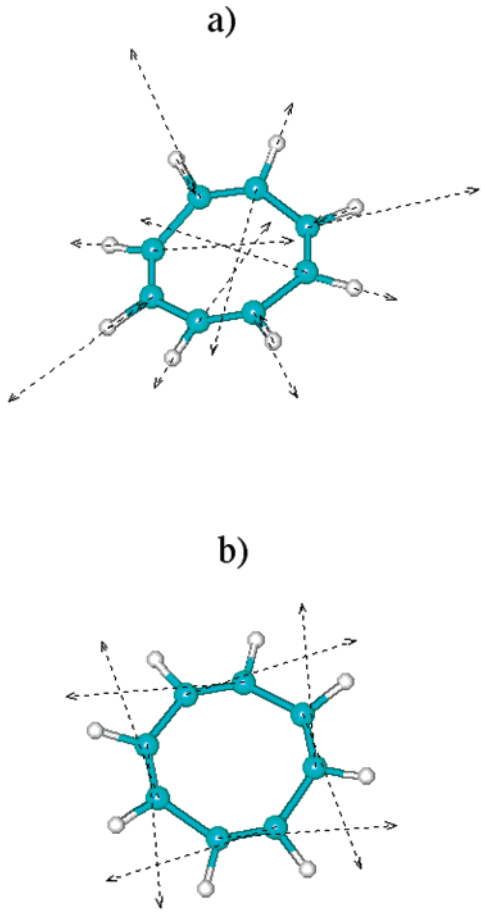

Figure 2. Gradient difference (a) and derivative coupling (b) vectors computed for the S_2/S_1 **CI** (see Figure 1) of D_{2d} symmetry.

(44) Klein, S.; Bearpark, M. J.; Smith, B. R.; Robb, M. A.; Olivucci, M.; Bernardi, F. *Chem. Phys. Lett.* **1998**, *292*, 259.
(45) Atchity, G. J.; Xantheas, S. S.; Ruedenberg, K. *J. Chem. Phys.* **1991**, *95*, 1862.

(46) Garavelli, M.; Page, C. S.; Celani, P.; Olivucci, M.; Schmid, W. E.; Trushin, S. A.; Fuss, W. *J. Phys. Chem. A* **2001**, *105*, 4458. Here we have reported how the dynamics through a conical intersection, if occurring along the lower-energy surface (as it is the case for motion through the first S_3/S_2 **CI**), must be accompanied by a change in the direction of motion which generally follows the derivative coupling vector. In this case, the computed derivative coupling vector (which possesses a C_{2v} symmetry) leads to D_{2d}-symmetry breaking. Therefore, it is likely that, after travelling through the first S_3/S_2 **CI**, the real motion of the system occurs along a D_{2d}-symmetry breaking path, which deviates from the D_{2d}-symmetric linear scan reported in Figure 1. Still, we suppose that this change is minor and insignificant for the discussion reported.

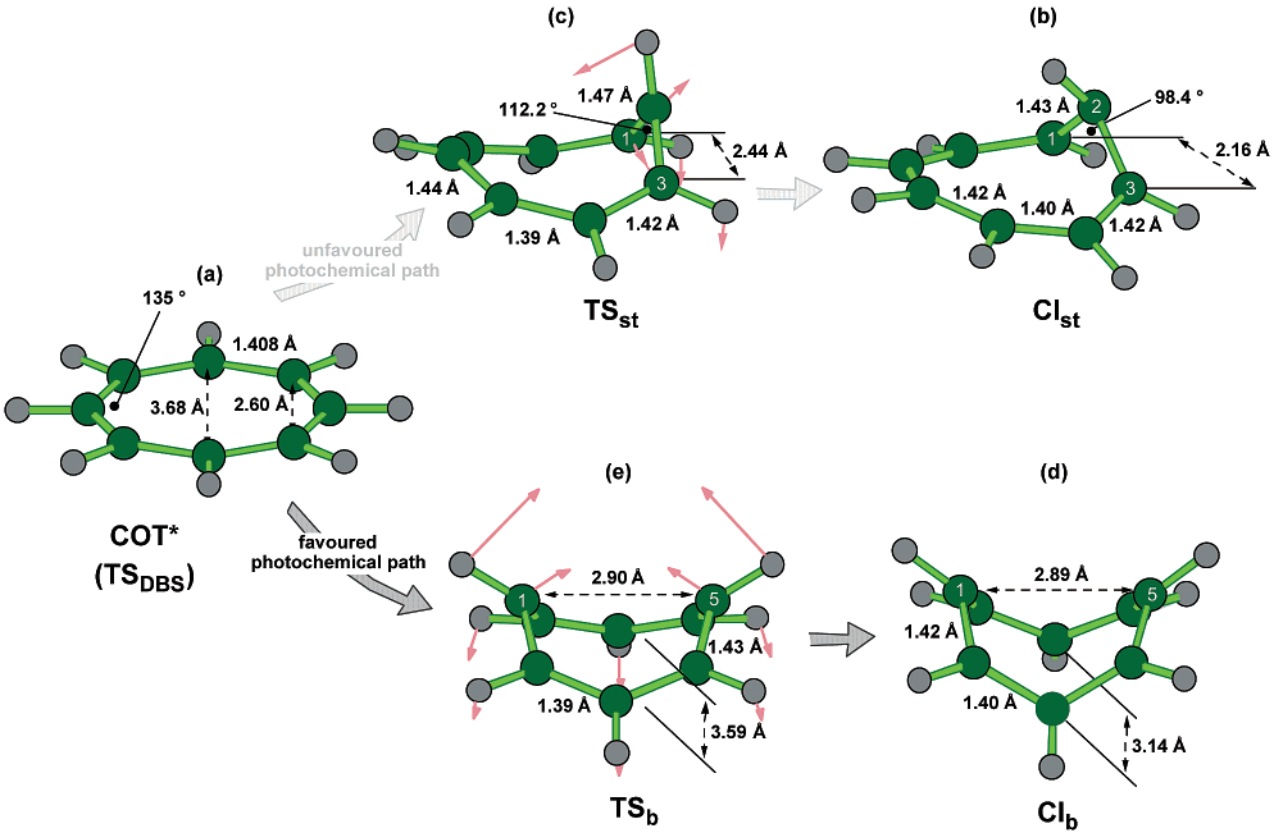

Figure 3. CASSCF/6-31G* optimized structures for **COT*** (**6**) (a), **CI$_{st}$** (b), **TS$_{st}$** (c), **CI$_b$** (d), and **TS$_b$** (e).

intersection has been shown[23−27] to prompt a common radiationless deactivation channel for photoexcited polyenes by providing the "funnel" for a fully efficient $S_1 \rightarrow S_0$ internal conversion (i.c.) and subsequent transformations (e.g., cis → trans photoisomerization and ring-closing reactions). **CI$_{st}$** is characterized by an unusual out-of-plane distortion: a triangular "kink" of a −CH−CH−CH− segment of the polyene chain (see Figure 3b). This $-(CH)_3-$ kink (whose central C_2 atom is pyramidalized) displays three weekly coupled π-electrons (see structure in Scheme 1) which are localized on three adjacent −CH− units, and a fourth electron which is delocalized along the remaining part of the cyclic conjugated system (a pentadienyl moiety).

The excited-state minimum energy path describing the **6** → **CI$_{st}$** reaction process goes through a high energy C_s-symmetric transition state (**TS$_{st}$**; see Figure 3c), which lies about 50 kcal/mol above **6** (see Table 2 and Scheme 1). The transition vector shown in Figure 3c describes the motion of the system on the way to **CI$_{st}$**. It is worth noting that, along this path, C_1 and C_3 approach each other (i.e., the C_1-C_3 distance shortens going from 2.60 Å in **6** to 2.16 Å in **CI$_{st}$**, and the $C_1-C_2-C_3$ bending angle reduces to 98°) with two unpaired (almost-localized) facing electrons. This will strongly affect the corresponding ground-state relaxation channels departing from **CI$_{st}$** (see section 3.3).

The **6** → **CI$_{st}$** path describes an energetically demanding process pushing the system toward a "standard" kinked conical intersection. However, as previously documented,[22] a different deformation drives the system toward a C_{2v}-symmetric boat form (see Scheme 1 and Figure 3d), decreasing the gap and making the crossing between the two potential energy surfaces possible. In this case, the system reaches an S_1/S_0 real crossing point (**CI$_b$**) at lower energy, which in fact represents the optimized *lowest energy* conical intersection for the system (see Table 2 for the energy differences). The computed minimum energy path driving the system towards **CI$_b$** appears to be easily accessible due to the moderate 15.2 kcal/mol energy barrier (PT2- and ZPE-corrected; see Table 2). This must be particularly true in the gas phase. Here, in fact, vibrational cooling and energy dissipation are much more inhibited than in the condensed phase, thus leaving the system with excess undissipated vibrational energy, which helps the molecule to easily overcome the barrier to **CI$_b$** (still leaving the path to **CI$_{st}$** less favored).

Analysis of the geometrical and electronic properties of **CI$_b$** indicates that it corresponds to a "quasi-tetraradical" system, with two unpaired opposite facing electrons placed in 1,5 relation on partially pyramidalized C centers (and two delocalized allyl systems in the remaining backbone). S_1 motion toward **CI$_b$** prompts 1,5 centers approaching (their distance shortens from 3.68 Å in **COT*** to 2.89 Å in **CI$_b$**); Figure 3e shows the geometrical structure and the transition vector associated with the optimized C_{2v} transition state (**TS$_b$**) along the **6** → **CI$_b$** path. (Because of root-flipping problems, **TS$_b$** optimization has been performed using state averaged orbitals (see Table 2).)

Scheme 1 reports the structures and the relative (to **COT***) PT2-corrected energies for all of the points discussed in this section.[47]

3.3. Photochemistry: The $S_1 \rightarrow S_0$ Deactivation Paths. Once the system reaches one of the two "tetraradicaloid" conical intersections, efficient $S_1 \rightarrow S_0$ internal conversion and branch-

(47) All PT2 computations give a well-balanced weight (0.76) for the CASSCF reference function in the first-order function. The reference PT2 absolute energy computed for **COT*** is −308.48067 au.

Scheme 2

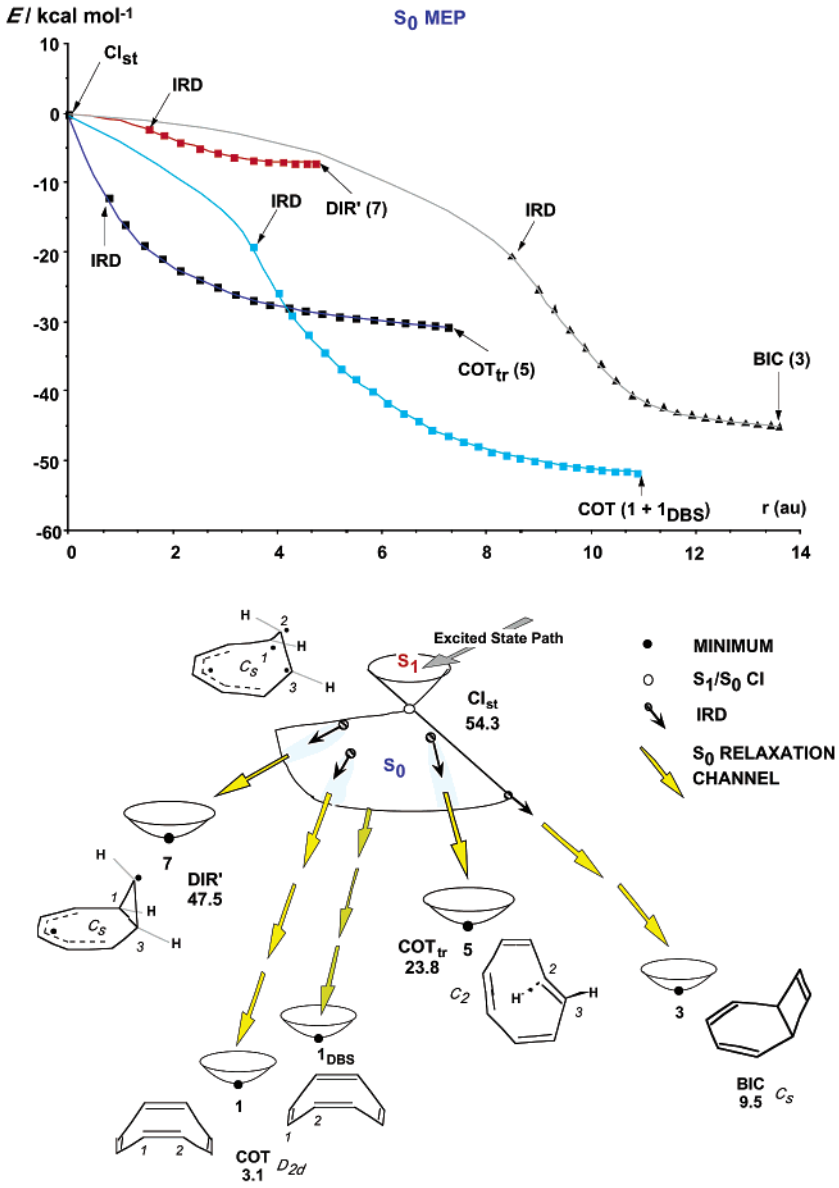

ing of the reaction channel occur.[28,29] In this section, we will analyze and discuss all of the possible relaxation paths departing from the tip of the two conical intersection points, the driving force for these processes being the electron recoupling of the highly unstable tetraradicaloid conical intersection structure. These channels have been computed via locating an initial direction of relaxation (IRD) on S_0, using an owner developed code (see section 2 and refs 31,32 for details).

Relaxation from CI_{st}. Two different IRDs have been located close to the higher-energy **CI_{st}** point, the first starting at 0.75 au (*mass-weighted* atomic units: amu$^{1/2}$ bohr) and the second at 1.5 au. Each IRD defines a minimum energy path leading towards a specific photoproduct: a strained cyclooctatetraene isomer (**COT_{tr}, 5**) of C_2 symmetry and a highly unstable bicyclic diradical intermediate (**DIR′**, **7**) of C_s symmetry, respectively (see Scheme 2 and Table 2 for the energetics).

Formation of photoproduct **7** occurs along a quite flat minimum energy path (MEP: see Scheme 2) which is the direct prolongation on S_0 of the motion gained by the molecule on S_1 along the **6** → **CI_{st}** reaction path (see the reactive mode displayed in Figure 3c). Although this path is not favored (i.e., it starts more distant and higher in energy; see Scheme 2), molecules may be channeled toward **7** if the momentum gained on the excited-state branch of the reaction coordinate is continued on the ground state. As documented in the previous section, this motion brings 1,3 C centers at a close proximity, leading to an increased overlap between the two facing localized π-orbitals (hosting two of the four unpaired electrons of the conical intersection point). Thus, if continued on S_0, a C_1-C_3 σ-bond formation process occurs to give intermediate **7** (see Figure 4a). Still, two unpaired electrons remain, thus making **7** a very unstable system. The first electron is localized on the pyramidalized apex of the cyclopropane ring (C_2), while the second is still delocalized on the pentadienyl moiety (see structures in Scheme 2). In section 3.4, we will document all of the thermal processes involving this very reactive intermediate.

Formation of photoproduct **5** (see Figure 4b) occurs via a cis → trans one-step isomerization process along a barrierless minimum energy path laying on the steeper side of the potential around the cone (see Scheme 2). Product **5** represents the

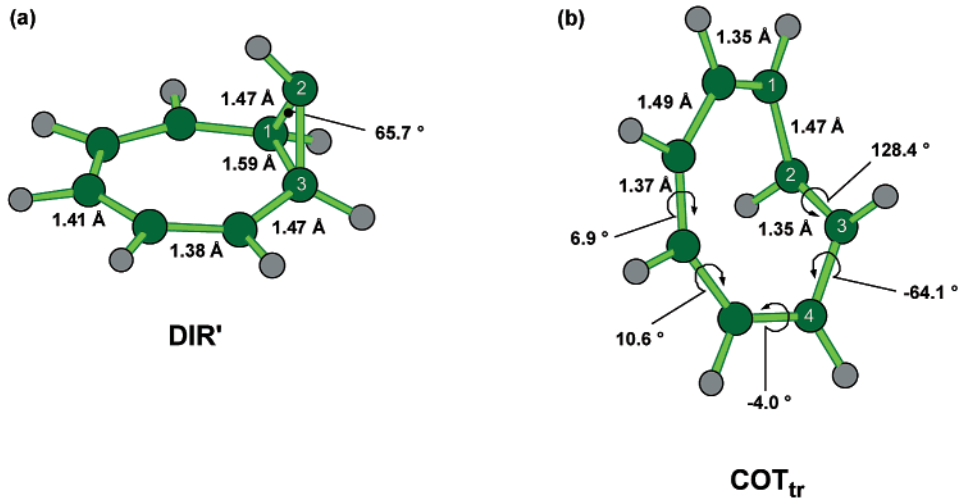

Figure 4. CASSCF/6-31G* optimized structures for **DIR′** (**7**) (a) and $\mathbf{COT_{tr}}$ (**5**) (b).

strained *trans,cis,cis,cis*-cyclooctatetraene isomer ($\mathbf{COT_{tr}}$) supposed by Zimmerman et al.[1] to be involved as an intermediate in the **1** → **2** photoconversion process (see eq d). Although energetically favored (the associated minimum energy path starting closer to $\mathbf{CI_{st}}$ and at a lower energy), its relaxation coordinate reveals that this channel requires a change in the direction of the excited-state motion (**6** → $\mathbf{CI_{st}}$). Thus, we can conclude that **7** may be formed (provided the system reaches $\mathbf{CI_{st}}$) for dynamic reasons (S_1 motion is continued on S_0 along the flat minimum energy path to **7**), even if **5** is energetically more favored.

Other two less favored IRDs have been located from the $\mathbf{CI_{st}}$ point. The first (at 3.5 au) is degenerate and leads back to the reactant (**1** and $\mathbf{1_{DBS}}$), and the second (at 8.5 au) drives the formation of the bicyclic isomer **3**. Although it has been shown[23−26,32] that disrotatory cyclobutene ring formation is easily prompted by decay via a $-(CH)_3-$ kinked conical intersection (see also section 4.2), still this process is very much unfavored in this case (and, in fact, the existence of this channel is doubtful, due to the big distance). This is due to the inverted direction of the pyramidalization found at carbon C2 (see Scheme 2), which favors trans double-bond coupling, on one hand, and puts geometric constraints to four-membered ring formation, on the other.

Relaxation from $\mathbf{CI_b}$. As previously documented,[22] the lowest energy conical intersection ($\mathbf{CI_b}$) corresponds to a "quasi-tetraradical" system, with two unpaired opposite facing electrons placed in 1,5 relation on partially pyramidalized carbon atoms (C_1 and C_5) and two allyl radicals in the remaining backbone. Again, recoupling between these four unpaired electrons characterizes ground-state relaxation. We have seen[22] that the S_1 reactive process **6** → $\mathbf{CI_b}$ promotes 1,5 centers approaching and prompts formation of a diradical intermediate with a C_1-C_5 transannular bond (see the reactive mode displayed in Figure 3e). The S_0 relaxation path corresponding to this process has indeed been located at a distance of 5 au from the conical intersection tip (see Scheme 3). The resulting C_{2v} bicyclo-[3.3.0]-octadienyl diradical (**DIR**; see Figure 5a) corresponds to the structure suggested by Iwamura et al.[48] and by Martin et al.[13] as the intermediate in the thermal valence isomerization of cyclooctatetraene to semibullvalene. **DIR** is a flat S_0 energy minimum at the CASSCF level, and, in fact, two very closed transition states of C_s symmetry ($\mathbf{TS_{CR}}$; see Figure 5b, and its symmetric − enantiomerically related − system) have been located at the CASSCF level, connecting the diradical to the two semibullvalene isomers **2** and **2′**. Yet, the inclusion of dynamic correlation energy (CASPT2 level; see Table 2) shows that this structure is unstable along the symmetry breaking motion which leads to $\mathbf{TS_{CR}}$ and to the C_s-symmetric semibullvalene (see Scheme 3 and Figure 5c). Thus, this structure turns out to correspond to the transition structure for the Cope rearrangement of semibullvalene, in agreement with previous works by Jiao et al.[20,21] and, more recently, by Castaño et al.[16] Therefore, there must exist a C_{2v}-symmetric bifurcation point[19] splitting the S_0 relaxation channel, which ultimately leads to the final photoproducts **2** and **2′** (i.e., the two possible semibullvalene isomers of the Cope rearrangement; see Scheme 3). These theoretical results are supported by studies of thermal isomerizations of substituted semibullvalenes and cyclooctatetraenes,[49−52] which reveal that the rates of Cope rearrangements and the **2** → **1** rearrangement are somehow correlated (see also section 3.4).

Besides representing an easily accessible channel for a fast internal conversion process, $\mathbf{CI_b}$ also promotes the branching of the reaction path. Other two degenerate and symmetric IRDs have been located in its proximity (1.5 au distance), whose minimum energy paths lead back to the D_{2d} reactant (**1**; see Figure 5d) or to its double-bond-shifted isomer ($\mathbf{1_{DBS}}$) (see Scheme 3). Although starting closer to the conical intersection and at a steeper side of the S_0 potential energy surface, analysis of the relaxation coordinate and comparison with the excited-state motion (**6** → $\mathbf{CI_b}$; see Figure 3e) reveal a drastic change in the direction of motion to populate these channels. Thus, we may conclude that semibullvalene formation is likely to occur for dynamic reasons (S_1 motion is continued on S_0 along the barrierless minimum energy path to semibullvalene), while cyclooctatetraene back recovery (and double-bond shifting) is favored for energetic reasons, so that both processes may be

(48) Iwamura, H.; Morio, K. *Bull. Chem. Soc. Jpn.* **1972**, *45*, 3599.
(49) Jackman, L. M.; Fernandes, E.; Heubes, M.; Quast, H. *Eur. J. Org. Chem.* **1998**, *2209*, 9.
(50) Quast, H.; Seefelder, M. *Angew. Chem., Int. Ed.* **1999**, *38*, 1064.
(51) Seefelder, M.; Quast, H. *Angew. Chem., Int. Ed.* **1999**, *38*, 1068.
(52) Quast, H.; Heubes, M.; Dietz, T.; Witzel, A.; Boenke, M.; Roth, W. R. *Eur. J. Org. Chem.* **1999**, *813*, 3.

Scheme 3

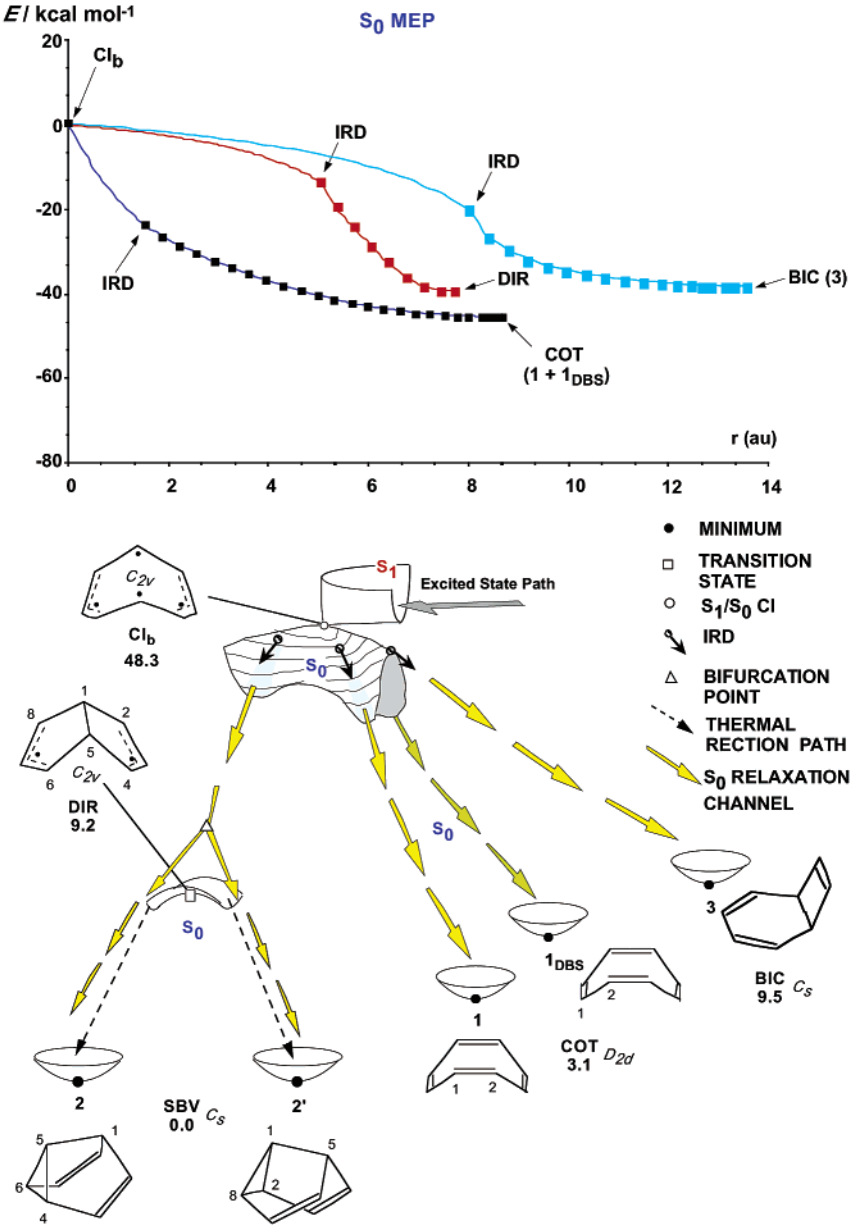

easily photoinduced, via suitably tuning reaction conditions. Remarkably, semibullvalene photoinduced formation has been observed to be more efficient in the gas phase[1] (i.e., dynamic control; see also section 4.1).

Finally, a fourth (unfavored) relaxation path has been located quite far from $\mathbf{CI_b}$ (8 au), which funnels a C_2-C_7 transannular σ-bond formation process leading to bicyclo-[4.2.0]-octa-2,4,6-triene (**3**). It is worth noting that, due to the big distance, doubts exist about a direct connection with $\mathbf{CI_b}$, and population of this deactivation channel (prompted by $\mathbf{CI_b}$ deactivation) seems to be quite difficult. Moreover, cyclobutene ring formation suggests a kinked conical intersection as a more suitable origin[23−26,32] (although with an inverted direction in the pyramidalization with respect to the one found at the carbon atom C2 in $\mathbf{CI_{st}}$). On the other hand, $\mathbf{CI_b}$ represents the only deactivation funnel easily accessible on S_1 by photoexcited cyclooctatetraene. In conclusion, although unfavored, still this path seems to be the only feasible route for isomer **3** photogeneration. This will allow us to explain concomitant benzene and acetylene formation following cyclooctatetraene irradiation (see section 4.4).[1] Finally, isomer **3** photogeneration may also be seen as involving cyclohexadiene ring formation. This is an alternative way to see the process. This photoinduced reaction has been widely investigated[32] and involves a decay from a conical intersection which is more similar to $\mathbf{CI_b}$ (due to the presence of an allyl radical) and which in fact resembles the relaxation path found from $\mathbf{CI_b}$ to **3**.

Because of the small **6** → $\mathbf{CI_b}$ activation barrier, internal conversion is very likely to occur via $\mathbf{CI_b}$. If this is the case, $\mathbf{CI_b}$ provides the rationale for cyclooctatetraene photochemistry (i.e., photoinduced semibullvalene formation and double-bond shifting) as we have previously shown.[22] Schemes 2 and 3 report structures and relative (to semibullvalene) PT2-corrected energies.[47]

3.4. Thermal Chemistry: S_0 Reaction Paths. Novel ground-state paths will be documented in the first subsection below,

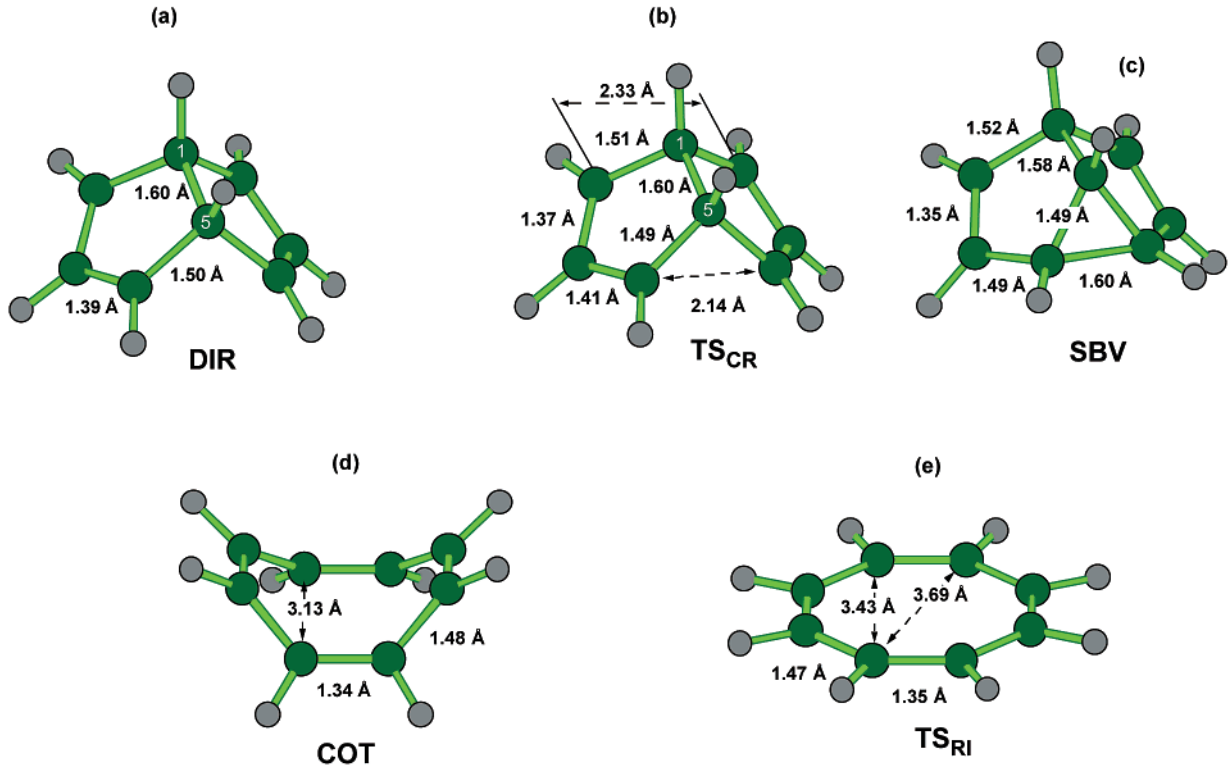

Figure 5. CASSCF/6-31G* optimized structures for **DIR** (a), **TS$_{CR}$** (b), **SBV** (**2**) (c), **COT** (**1**) (d), and **TS$_{RI}$** (e).

which connect **CI$_{st}$** and **CI$_{b}$** photoproducts. In addition, also previously studied thermal processes (i.e., valence isomerization, Cope rearrangement, ring inversion, and double-bond shift) have been reinvestigated here to have both an improved energetic (via PT2 computations) and a homogeneous full-comprehensive reactivity scheme embracing the full network of excited-state and ground-state reaction channels. Finally, these results will be used for comparison with the available experimental data. The good agreement shown below provides a validation for the computational method employed.

Thermal Paths Interconnecting CI$_{st}$ and CI$_{b}$ Photoproducts. As shown in section 3.3, intermediate **7** is very unstable and highly reactive. Provided it is formed, the cyclopropane ring easily opens (i.e., breaking of the previously formed 1,3 C−C σ bond), promoting a 2,3 π-orbitals coupling (which restores the octagonal π-system). This process involves an asymmetric low-energy barrier transition state (**TS$_{DIR'}$**; see Figure 6a and Table 2). Thus, **TS$_{DIR'}$** connects **7** to **5** (see Scheme 4); isomer **5** is formed due to the pyramidalization of C_2, which in fact favors a trans-double-bond coupling. Therefore, a minimum energy path exists which connects the two possible photoproducts (**7** and **5**) directly generated via deactivation through **CI$_{st}$** (see section 3.3). Anyway, another interesting transformation (all along a C_s-symmetric minimum energy path) may involve **7**; via a coupling of the two left unpaired electrons, a **7** → **2** conversion occurs. At the CASSCF level, this process is a two-step reaction (see Table 2 for the energetics). First, **7** is converted to its isomer **DIR″** (Figure 6c) via the transition state **TS′**, (Figure 6b) which corresponds to a C_2-pyramidalization inversion process. Second, C_2−C_6 σ-bond formation occurs to give semibullvalene via the transition state **TS$_{SBV}$** (Figure 6d). Anyway, PT2 corrections show that this process corresponds to a single-step reaction (as shown in Scheme 4) with a unique transition state (**TS$_{SBV}$**), the structures **7**, **TS′**, **DIR″**, and **TS$_{SBV}$** being of increasing energy, respectively (see Table 2). Scheme 4 reports also the relative (to semibullvalene) PT2-corrected energies.[47]

Cope Rearrangement. The bicyclo-[3.3.0]-octadienyl diradical (**DIR**) has already been recognized as the transition state for Cope rearrangement (see section 3.3) between the two semibullvalene isomers **2** and **2′**, as previously pointed out by the work of Jiao et al.[20,21] and Castaño et al.[16] The PT2- and ZPE-corrected barrier for Cope rearrangement is 6.9 kcal/mol, very close to the experimental value of 5.5 kcal/mol[15] and the recently computed value of 6.0 kcal/mol.[16]

Valence Isomerization. Castaño et al.[16] have recently investigated the reversible semibullvalene to cyclooctatetraene valence isomerization process (see eq h), calculating a barrier of 47.4 kcal/mol for **2** → **1** interconversion and locating a bifurcation point[16,19] along the minimum energy path downhill from the C_2 transition state (**TS2$_{VI}$**; see Figure 7a) toward the two semibullvalene isomers **2** and **2′**; see Scheme 5. Here, we have computed (PT2 plus ZPE corrections) a significantly smaller barrier for this process (37.6 kcal/mol), in much better agreement with the reported 39.8 kcal/mol experimental value.[14] Moreover, we have found that, although very close in energy, **2** is slightly more stable than **1** (only a 1.3 kcal/mol separation; see Table 2). Anyway, energy separation is below PT2 errors (around 1−2 kcal/mol), so that no conclusive statement may be inferred. We have also reinvestigated the second (energetically more favored) valence isomerization process involving **1** → **3** interconversion (for a previous computational study, see ref 18). The computed (PT2- and ZPE-corrected) energy barrier for the corresponding C_s-symmetric transition state (**TS1$_{VI}$**; see Figure 7b) is 26.9 kcal/mol, very close to the experimental value

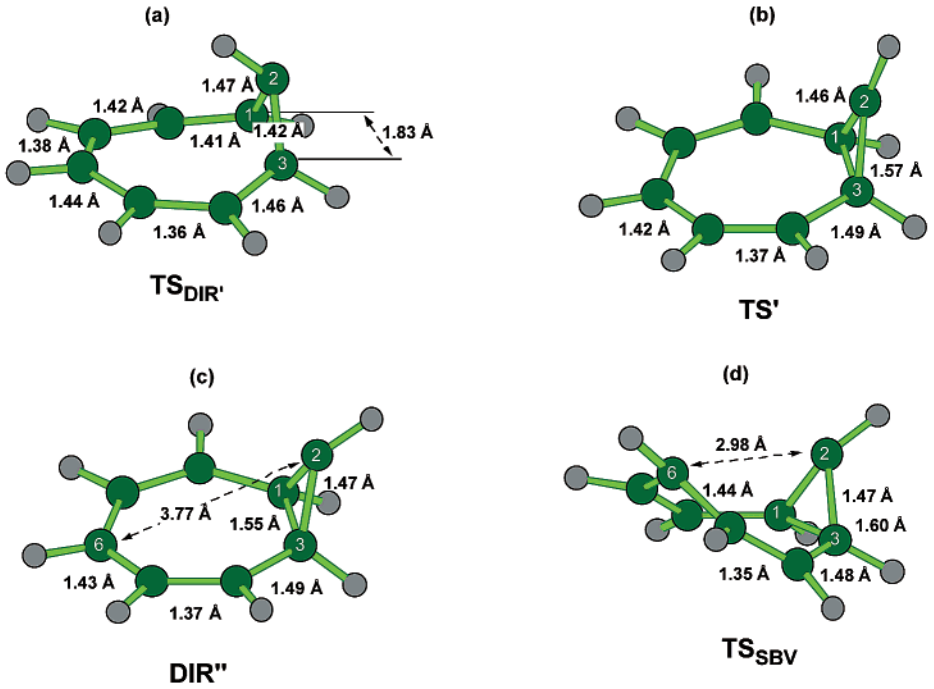

Figure 6. CASSCF/6-31G* optimized structures for **TS$_{DIR'}$** (a), **TS′** (b), **DIR′′** (c), and **TS$_{SBV}$** (d).

Scheme 4

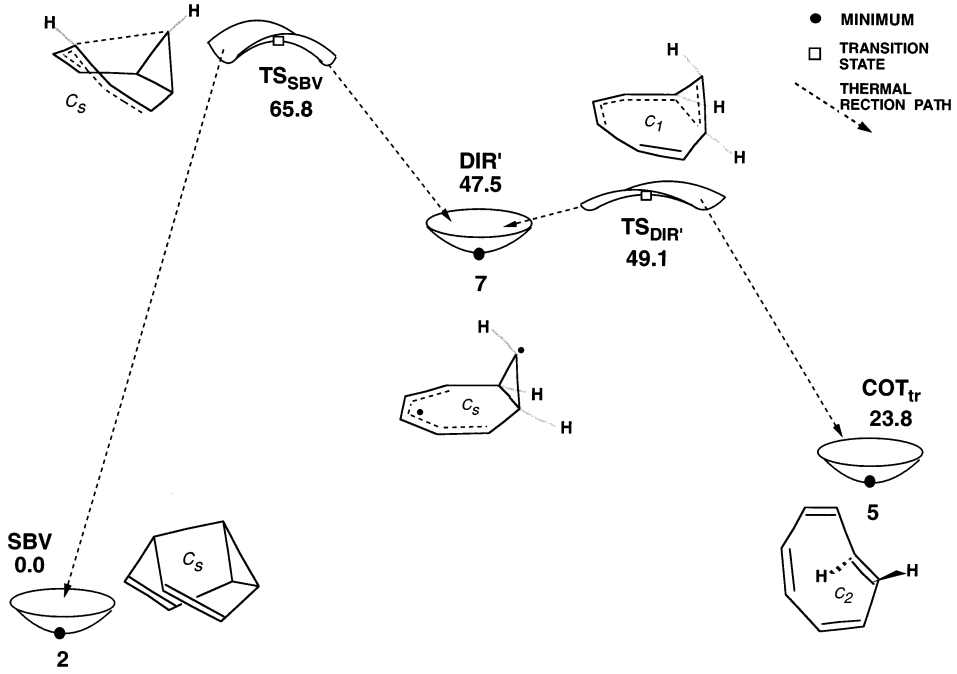

of 28.1 kcal/mol.[12] Geometry of **3** is shown in Figure 7c. Scheme 5 reports also the relative (to semibullvalene) PT2-corrected energies.[47]

The mechanistic picture displayed in Scheme 5 is supported by recent experimental observations for the thermal isomerizations of substituted semibullvalenes and cyclooctatetraenes.[49−52] Interestingly, Quast et al. have shown that the rates for the Cope and the **2** → **1** rearrangements are somehow correlated. These findings nicely fit with the theoretical results documented here and in ref 16 and can be easily interpreted in terms of the potential energy surface reported in Scheme 5. Moreover, formation of two noninterconvertible double-bond shifting isomers of a highly substituted cyclooctatetraene (compounds 14b and 15b in ref 52) has been described. These compounds very likely arise from two isomeric transition structures of the **TS2$_{VI}$**-type. Obviously, in the thermal rearrangements of semibullvalenes, one bifurcation point exists for each single **TS2$_{VI}$**-type transition state.

Double-Bond Shifting and Ring Inversion. As stated in the Introduction, thermal cyclooctatetraene double-bond shifting (**1** → **1$_{DBS}$**) and ring inversion (**1** → **1′**) have been widely investigated both experimentally and computationally.[3−7] These studies have lead to energy barriers of about 14 and 10 kcal/mol[8−11] for the associated transition states, **TS$_{DBS}$** and **TS$_{RI}$**, respectively (see Figures 3a and 5e). As previously shown by Borden,[3−5] CASSCF may properly describe these processes. In

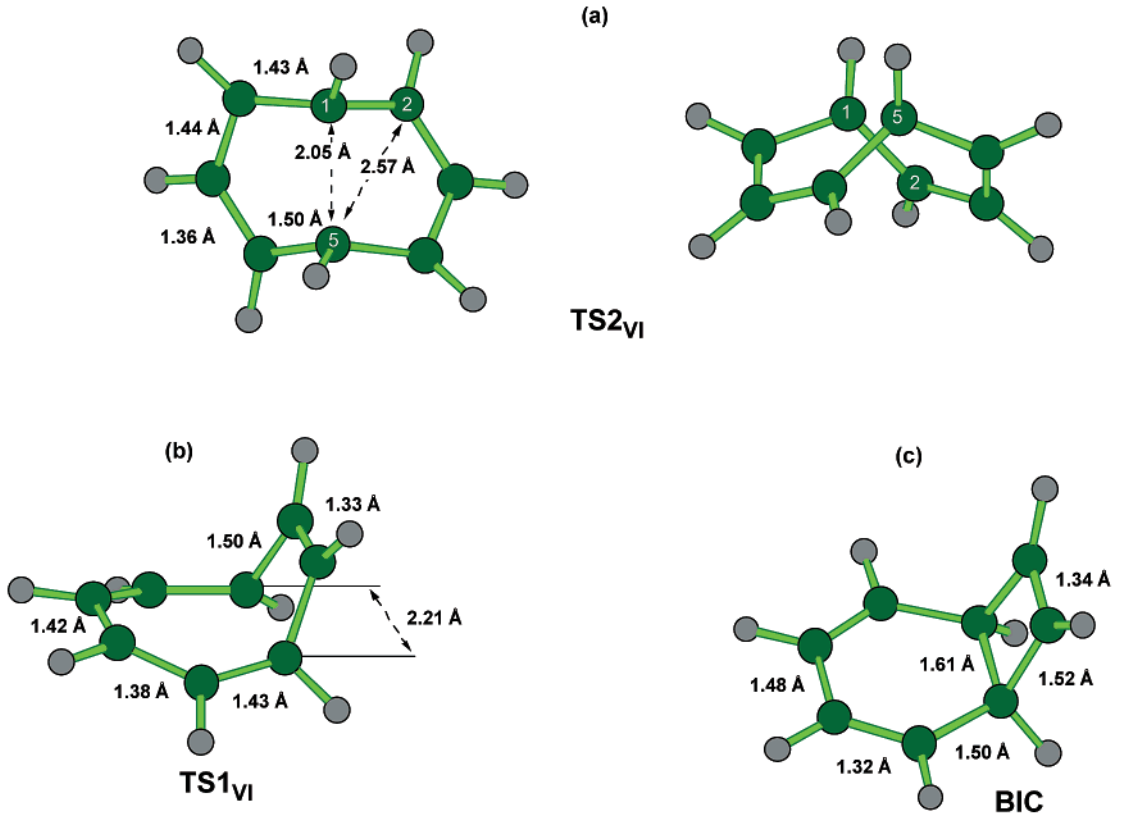

Figure 7. CASSCF/6-31G* optimized structures for **TS2$_{VI}$** (a), **TS1$_{VI}$** (b), and the bicyclo-[4,2,0]-octa-2,4,7-triene **BIC** (**3**) (c).

Scheme 5

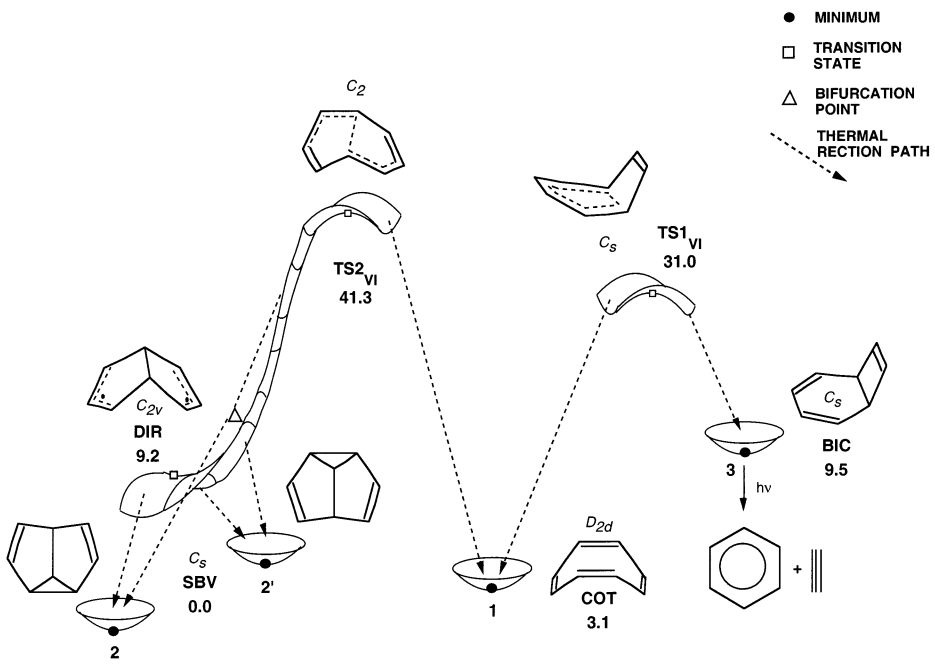

fact, via CASSCF/6-31G* optimizations (plus ZPE corrections), we calculate energies which are in very good agreement both with previous computations[3−5] and with experiments:[8−11] 14.5 and 10.9 kcal/mol, respectively (see Table 2). Anyway, when correcting for dynamic correlation (PT2 values in Table 2), the two transition states come very close in energy (about 13 kcal/mol both). They even invert their order, **TS$_{DBS}$** being lower (11.0 kcal/mol) than **TS$_{RI}$** (12.9 kcal/mol), when we include ZPE corrections. Yet, the energy difference is within the expected error bars of the CASPT2 method. Analysis of the optimized double-bond shifting transition structure (**TS$_{DBS}$**) reveals that it has exactly the same geometry as the relaxed planar D_{8h}-symmetric minimum found on S_1 (**6**, **COT***) and shown in Figure 3a. Provided we consider this point (**TS$_{DBS}$**) higher in energy (as the CASSCF results[3−5] and the experimental data[8−11] show; see also Table 2), a D_{4h}-symmetric bifurcation point is easily predicted along the path connecting **TS$_{DBS}$** to the cyclooctatetraene product wells. This point splits the minimum

Scheme 6

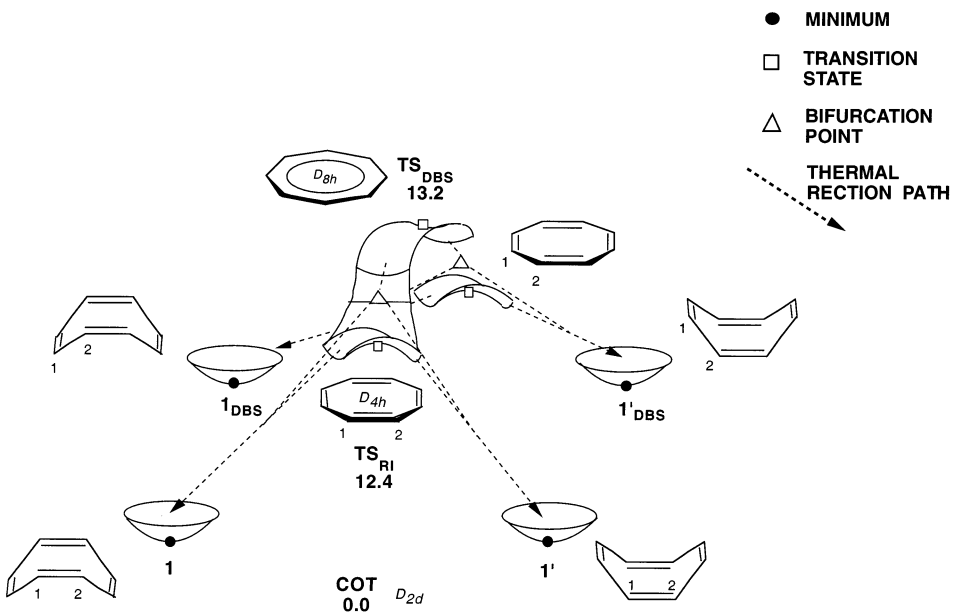

energy path into two branches, ultimately leading toward the two possible ring-inverted cyclooctatetraene isomers (**1** and **1′**), thus avoiding the lower lying transition state for ring inversion ($\mathbf{TS_{RI}}$). Scheme 6 depicts this situation, reporting also the structures and relative (to cyclooctatetraene) PT2-corrected energies. This picture has been recently fully confirmed by the work of Castaño.[19b]

4. Discussion

4.1. Dynamics versus Energetic Control: Vibrationally "Hot" and Vibrationally "Cold" Photochemistry. In section 3.3, we have shown that the semibullvalene relaxation path departing from $\mathbf{CI_b}$ is, substantially, the continuation (through $\mathbf{CI_b}$ and **DIR**) of the S_1 path. Anyway, the two additional degenerate relaxation paths also originating in the proximity of $\mathbf{CI_b}$ and leading back to the reactant (**1**) and to its double-bond shifting isomer ($\mathbf{1_{DBS}}$) are energetically more favored because they begin closer (1.5 au distance) to the $\mathbf{CI_b}$ point and develop along steeper regions of the S_0 energy surface (see Scheme 3). Furthermore, their relaxation coordinate indicates that, with respect to the S_1 transition vector (see Figure 1e) and in contrast to the semibullvalene path, a drastic change in the direction of "motion" is needed to populate these paths.

The above results do not provide evidence for the formation of the previously proposed[1] *trans*,*cis*,*cis*,*cis*-cyclooctatetraene (**5**) as an intermediate for the two-photon generation of semibullvalene. Although such a structure has been shown to be formed via deactivation through $\mathbf{CI_{st}}$ (see section 3.3), still this path has been located much higher in energy to provide a competitive deactivation funnel for photoexcited cyclooctatetraene.

Interestingly, the documented S_0 relaxation paths provide a computationally based model for predicting the products observed in either vibrationally hot or vibrationally cold cyclooctatetraene photochemistry.[1,2] In the case of a low amount of S_1 vibrational excess energy, **COT*** would reach the $\mathbf{CI_b}$ region with a small momentum along the reactive mode shown in Figure 3. In these conditions, decay to S_0 would result in the population of the closer and steeper relaxation paths, yielding

Scheme 7

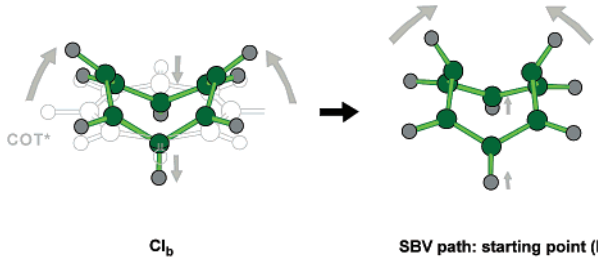

ground-state cyclooctatetraene together with its double-bond shift tautomer only. This interpretation has been validated in our previous work on cyclohexadiene/hexatriene photoinduced interconversion.[32] On the other hand, in the presence of a vibrationally excited reactant, at least part of the S_1 population will be channeled along the transition vector with enough momentum to be displaced toward the semibullvalene relaxation path. As a consequence, the photolysis of cyclooctatetraene would yield a mixture of semibullvalene and double-bond-shifted cyclooctatetraene photoproducts. This model seems to provide an explanation for the fact that semibullvalene can be efficiently produced in the gas phase (vibrationally hot) photolysis of cyclooctatetraene.[2] This model would also explain the low photochemical reactivity displayed by polysubstituted cyclooctatetraenes such as 1,3,5,7-tetramethyl-cyclooctatetraene, which does not lead to a detectable production of 1,3,5,7-tetramethyl-semibullvalene.[1] This would be the result of a mass effect due to the 1,3,5,7-substituents. In fact, because a significant displacement of these substituents is needed to boost population along the semibullvalene relaxation channel (i.e., $\mathbf{COT^* \rightarrow CI_b \rightarrow SBV}$ path; see Scheme 7), increasing the mass of the substituents (i.e., replacing four hydrogen atoms in cyclooctatetraene) will clearly slow this motion. Thus, inertia and steric factors would favor reactant back formation and double-bond shifting. Moreover, for a polysubstituted cyclooctatetraene (such as 1,3,5,7-tetramethyl-cyclooctatetraene), the paths to the lowest energy conical intersection (the $\mathbf{CI_b}$ equivalent) could even be higher in energy, restraining this channel and, consequently, semibullvalene photogeneration.

Scheme 8

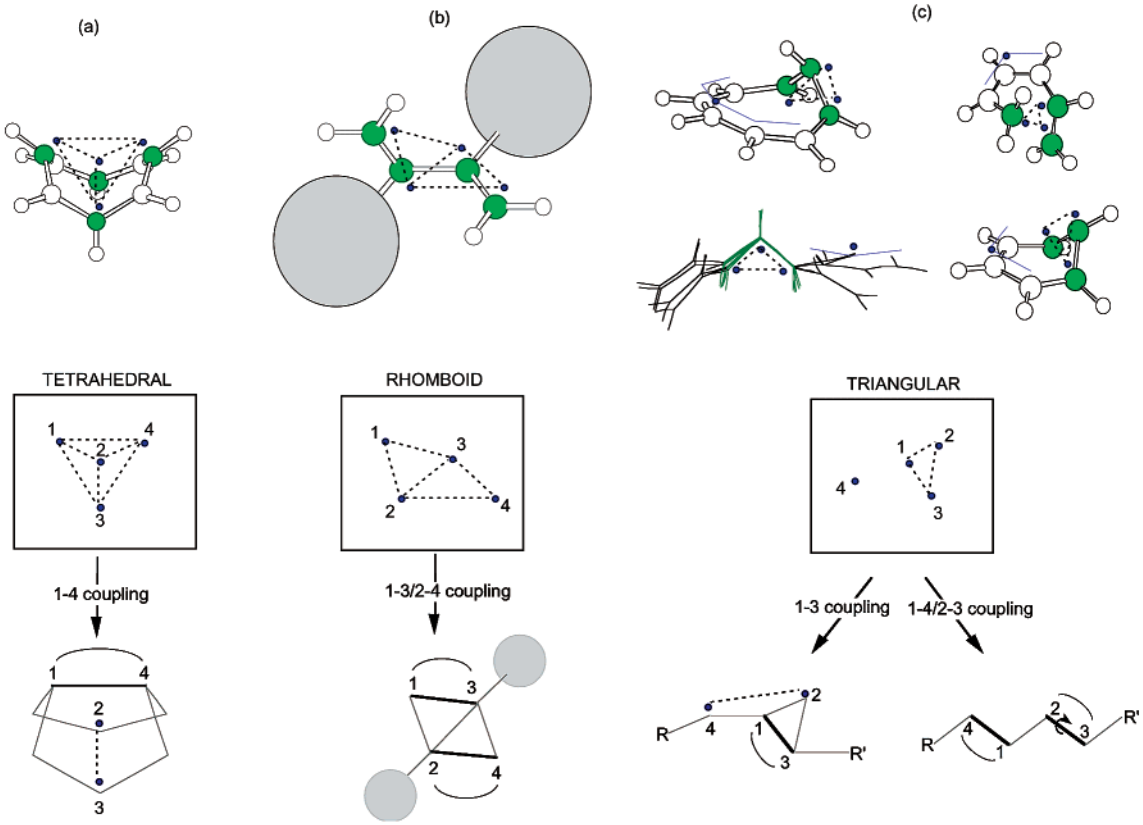

Finally, it is worth noting that double-bond shifting (and reactant back formation) may also arise via radiative/nonradiative vertical decay from structure **6** (the S_1 D_{8h}-symmetric **COT***). We have seen that **6** is identical to the transition state for double-bond shifting (**TS_{DBS}**), which is about 20 kcal mol^{-1} lower in energy. Therefore, cyclooctatetraene deactivation would result in a **6** → **TS_{DBS}** process, which populates the thermal double-bond shifting channel and favors double-bond shift versus semibullvalene formation even more. This decay route is favored in conditions (such as in a cold environment) where the system does not have enough energy to be channeled toward the low-energy conical intersection (**CI_b**) and/or the corresponding energy barrier is too high (as it may occur for some polysubstituted cyclooctatetraenes).

4.2. Prototype Conical Intersections in Conjugated Hydrocarbons. We have provided evidence that the photochemical behavior of cyclooctatetraene is dominated by the presence of a boat-shaped conical intersection funnel (**CI_b**), featuring a new type of molecular and electronic structure, as previously documented in our work.[22] The analysis of this point shows that **CI_b** has a tetraradical character with two unpaired electrons located on two opposite centers (atoms C_1 and C_5) and the other two electrons residing on the allyl moieties $C_2-C_3-C_4$ and $C_6-C_7-C_8$ (see Scheme 8a). In the past,[53] the same pattern and conical intersection have been documented for the case of the H_4 clusters. For these elementary systems, other two geometric and electronic arrangements have been documented for conical intersections, according to different tetraradical-type interaction patterns such as rhomboid (Scheme 8b) and triangular (Scheme 8c), respectively. While **CI_b** represents the first example found until now in conjugated hydrocarbons for a tetrahedral interaction scheme in low-energy conical intersections, the other two patterns have the equivalent in previously optimized structures. For example, the four unpaired electrons of the low-energy conical intersections found in 2,3-di-*tert*-butyl-buta-1,3-diene[27] and in the ethylene−ethylene cycloaddition[31] interact according to a rhomboid pattern (see Scheme 8b), while benzene, cyclohexadiene, and linear conjugated chains in general have triangular-type low-energy conical intersections (see Scheme 8c).[23−26,32] As is clearly shown in Scheme 8, each prototype conical intersection has its specific recoupling scheme on the ground state. Thus, a rhomboid pattern may prompt the simultaneous formation of two new σ-bonds (leading to bicyclobutane via a one-step concerted mechanism).[27] On the other hand, $-(CH)_3-$ kinked intersections may prompt both cis → trans photoisomerizations and 1,4/1,3 σ-bond formations (leading, for example, to cyclopropanation reactions), as seen in benzene, cyclohexadiene, linear polyenes,[23−26,32] and cyclooctatetraene (photoinduced formation of intermediate **7** from **CI_{st}**). Finally, tetrahedral interaction at the boat conformer of **CI_b** promotes C_1-C_5 transannular bond formation, leading to the unstable diradical intermediate **DIR**.[22]

A major task in our study is to understand and rationalize the factors playing a role in the selection and stability of low-energy conical intersections. As discussed above, each structure controls the outcome of a photochemical process. The knowledge of a simple predictive model could provide valuable guidelines for designing selective photochemical processes leading to complex molecular architectures (e.g., polycyclic carbon backbones) through irradiation of simple conjugated

(53) Gerhartz, W.; Poshusta, R. D.; Michl, J. *J. Am. Chem. Soc.* **1977**, *99*, 4263.

Scheme 9

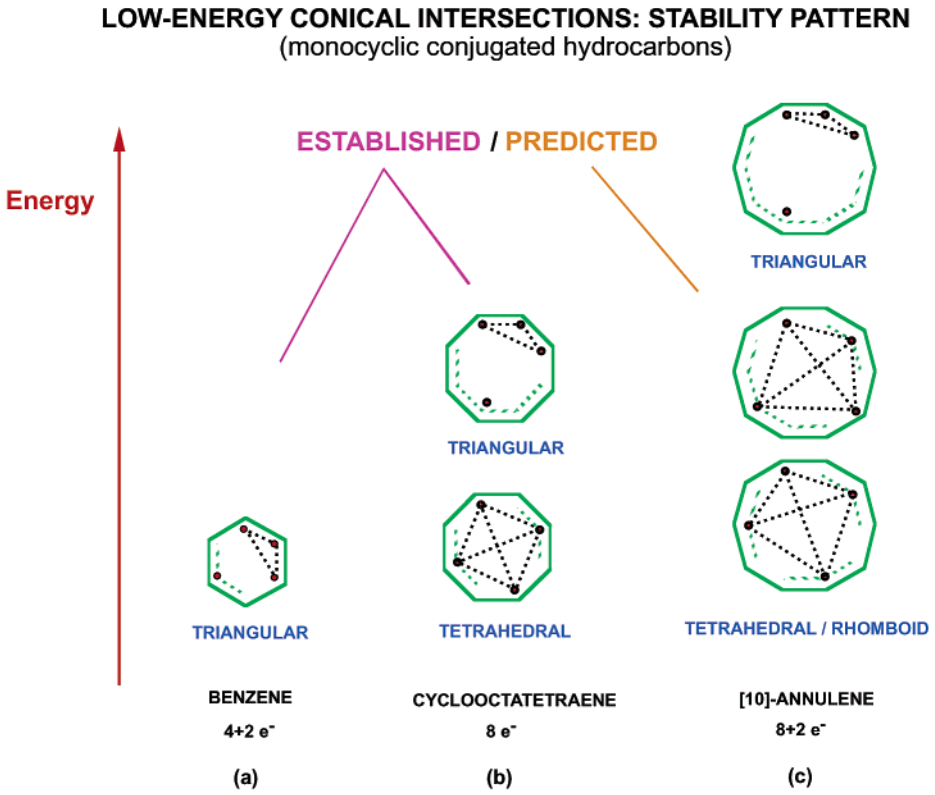

hydrocarbons.[54] Examples of these processes are the production of bicyclobutanes from butadienes,[55] tetrahedranes from cyclobutadienes,[56] benzvalenes from benzenes,[57] and semibullvalenes from cyclooctatetraenes.[1,2,58] An example comes from our previous work on (substituted or unsubstituted) butadiene photochemistry.[27] Here, we have shown how steric effects (as the ones caused by strategically placed bulky *tert*-butyl substituents) may control the outcome of the photochemical process, selecting the prototype (triangular or rhomboid) conical intersection funnel involved in the reaction. Cyclooctatetraene allows us to extend this investigation also to electronic factors. A simple question may help us to catch the issue: why cyclic systems such as benzene (an aromatic hydrocarbon) and cyclohexadiene (and in general linear conjugated hydrocarbons) decay through a low-energy $-(CH)_3-$ kink conical intersection, while in cyclooctatetraene this point (i.e., $\mathbf{CI_{st}}$) is very high in energy and the favored reactive funnel corresponds to a different prototype (tetrahedral) crossing ($\mathbf{CI_b}$)?

An answer may be found for conjugated cyclic systems via the examination of all of the possible *low-energy* covalent valence-bond (VB) configurations, arranging the four unpaired electrons of a conical intersection. While for benzene (as well as cyclohexadiene) the lower-energy arrangement may only involve *one* delocalized allyl radical and *three* adjacent unpaired electrons (i.e., the triangular kink, see Schemes 8c and 9a), in cyclooctatetraene, due to its larger size, a new and more stable tetraradical-type configuration is possible. This configuration corresponds to the electronic structure found in $\mathbf{CI_b}$ and accommodates a tetrahedral interaction pattern (see Scheme 8a). Here, we have only *two* unpaired single-centered (C_1, C_5) electrons, plus *two* delocalized allyl radicals (see Scheme 9b). Obviously, this configuration is electronically more favored than the kinked (triangular) one ($\mathbf{CI_{st}}$), where three unpaired electrons are localized on adjacent carbon centers (C_1, C_2, C_3), and only one delocalized radical exists. Thus, in conclusion, it appears that the existence of different covalent configurations depends on the extension of the system and, in turn, on the energy of the orbitals which accommodate the electrons.

By further extending the length of the ring (e.g., to cyclodecapentaene), we could end up with an even more stable tetraradical-type configuration for a conical intersection. This involves, according to our model, a four-centered interaction pattern with *three* singly occupied allyl orbitals and only *one* singly occupied carbon-centered π-orbital (see Scheme 9c). A second less stable configuration involves only *two* delocalized (an allyl and a pentadienyl) radicals and may generate a higher-energy conical intersection structure. Finally, a third unstable configuration (with only *one* delocalized heptatrienyl radical) matches a triangular pattern and therefore corresponds to the most unstable $-(CH)_3-$ kink crossing point. Provided these electronic effects are the only interactions involved (e.g., steric interactions are ca. equivalent for the different conical intersections), we should end up with the energetic order shown in Scheme 9c. On the other hand, unsubstituted linear conjugated systems (e.g., all-trans polyenes) can reach (from their side of the potential) only triangular-type conical intersections (i.e., the $-(CH)_3-$ kinked crossing). For the other interaction patterns to occur, major conformational changes are necessary.

Although qualitative, this picture seems to fit experimental and computational evidence and could be of predictive value

(54) Gilbert, A. In *CRC Handbook of Organic Photochemistry and Photobiology*; Horspool, W. M., Song, P.-S., Eds.; CRC Press: Boca Raton, FL, 1995; pp 229−236.
(55) Hopf, H.; Lipka, H.; Traetteberg, M. *Angew. Chem., Int. Ed. Engl.* **1994**, *33*, 204.
(56) Maier, G. *Angew. Chem., Int. Ed. Engl.* **1988**, *27*, 309.
(57) Bryce-Smith, D.; Gilbert, A. *Tetrahedron* **1976**, *32*, 1309.
(58) Zimmerman, H. E.; Grunewald, G. L. *J. Am. Chem. Soc.* **1966**, *88*, 183.

in the photochemistry of conjugated hydrocarbons. Moreover, this model may help us both to design and to control ad hoc photoinduced processes; via tuning the conditions which affect the stability of VB configurations (and therefore the related conical intersection structures), it could be possible, in principle, to select among different photoproducts patterns.

Accurate investigation of larger terms (such as cyclodecapentaene and longer polyene chains), complemented by exploration and characterization of the S_1/S_0 intersection space (i.e., the *n*-2-dimensional degenerate space), may shed new light into this fascinating area.

Finally, it is worth noting that in cyclooctatetraene, the energy barriers to $\mathbf{CI_b}$ and $\mathbf{CI_{st}}$ (15.2 and 44.0 kcal mol^{-1}, respectively) are significantly bigger than the ones computed for low-energy conical intersections in other conjugated systems such as benzene (∼9 kcal mol^{-1}), cyclohexadiene (<1 kcal mol^{-1}), and linear chains. In fact, relaxed S_1-excited cyclooctatetraene (**COT***) has an extended delocalized structure (i.e., identical 1.40 Å π-bonds and planarity, recalling an aromatic system). Therefore, we can think about **COT*** as being stabilized by a kind of aromatic effect which plays against the out-of-plane deformation needed to reach both the boat ($\mathbf{CI_b}$) and the kink ($\mathbf{CI_{st}}$) structures (because this motion breaks delocalization, and stabilization effects are lost). This feature makes the paths to out-of-plane crossing points more demanding in energy than for the other conjugated systems, which do not display such a stabilization effect on S_1. While this is obvious for linear polyenes, also relaxed S_1-excited benzene (which corresponds to an anti-Kekule minimum with long − 1.43 Å − π-bonds)[26] has partially lost its aromatic stabilization. Therefore, in general, radiationless decay routes via conical intersections are lower in energy for these systems.

4.3. Cyclooctatetraene as a Double-Bond Shifting Device for Photoswitches. Section 4.1 shows that photoinduced SBV formation and double-bond shifting are intrinsically competitive processes, as these are prompted by decay at the *same* conical intersection funnel ($\mathbf{CI_b}$). This conclusion seems to impose severe limitations to the practical use of cyclooctatetraene for the construction of molecular switches or other types of photoswitchable devices. Anyway, we have seen how tuning reaction conditions (e.g., condensed/gas phase, reaction temperature, etc.) and/or substitutions (e.g., polysubstituted cyclooctatetraene) may heavily affect relaxation paths and final photoproducts. For instance, in solution or in a cold matrix, where the excess vibrational energy is rapidly removed (i.e., in condition of low vibrational excess energy), the double-bond shifting process should dominate. In fact, if the system reaches $\mathbf{CI_b}$ with a small momentum (e.g., a vibrationally cold system), or if it does not have enough energy to be channeled along the path (so that it decays radiatively/nonradiatively from **COT***), and/or if the energy barrier is too high (as it may occur in some polysubstituted cyclooctatetraene), decay to S_0 would yield reactant back formation and double-bond shift isomer only. Therefore, under these conditions, it should be possible, in principle, to favor double-bond shifting versus competitive semibullvalene photogeneration.

A general cyclooctatetraene-based molecular switch has at least two vicinal substituents (see eq f). As seen in section 4.1, substitution may lock semibullvalene formation so that (even in a very simple switch) photoinduced double-bond shifting is favored. This effect should be enhanced as the number of substituents increases. Provided the basic photochemical properties of cyclooctatetraene-based systems remain the same (i.e., the qualitative shape of the potential energy surfaces involved does not change), we may conclude that photochemically controlled double-bond shifting can be used to design cyclooctatetraene-based molecular switches. In particular, if the "on-state" (see eq f) absorbs at a different wavelength than the "off-state" (which is likely to occur for π-substituents), it should be possible, in principle, to specifically control the conversion of one isomer to the other, and vice versa.

4.4. Benzene and Acetylene Byproducts Photogeneration. In section 3.3, we have seen how a competitive (but less favored than **COT** and double-bond shifting) bicyclo-[4.2.0]-octa-2,4,6-triene (**3**) photogeneration may occur along an additional relaxation path from $\mathbf{CI_b}$, leading to C_2-C_7 transannular bond formation. Product **3** may then absorb a second photon to give benzene and acetylene[1] (eq b), which in fact have been observed as concomitant byproducts in cyclooctatetraene irradiation experiments (see eq a).[1] This two-photon mechanistic explanation for concomitant benzene and acetylene formation seems to be more realistic than the one involving a photochemically induced two-step process for the generation of intermediate **3**. This process corresponds to hot-cyclooctatetraene recovery (from **COT*** internal conversion) followed by thermal **1** → **3** valence isomerization. Anyway, benzene formation is mainly observed in condensed-phase experiments at low temperatures,[1] where generation of hot-reactant and intermediate **3** (via thermal **1** → **3** valence isomerization) should be very unlikely to occur. Under these conditions, a process (even if it is less favored) directly generating **3** from $\mathbf{CI_b}$ deactivation is certainly preferred.

5. Conclusions

Computational evidence shows that evolution of photoexcited cyclooctatetraene out of the FC region prompts an efficient radiationless decay of the bright S_2 (^{1}E) state into the dark lowest S_1 ($^1A_1$) state, leading to population of a planar D_{8h} excited minimum **COT***. Nonadiabatic transitions to S_0 appear to be controlled by two different tetraradical-type conical intersections ($\mathbf{CI_{st}}$ and $\mathbf{CI_b}$), directly connected to **COT*** by excited-state reaction paths. Electronic factors playing a role in the stability and selection of low-energy conical intersection funnels have been analyzed, and a crude qualitative model has been elaborated, which allows prediction for the electronic structure of low-energy crossings in unsaturated cyclic systems. $\mathbf{CI_{st}}$ belongs to the family of the $-(CH)_3-$ kinked crossings found in smaller cyclic terms and linear polyenes; it prompts ground-state relaxation channels leading both to three- (or four-) membered ring formation (**7**, **3**) and to cis → trans isomerization (**5**) (i.e., the typical photoproducts observed from $-(CH)_3-$ kinked intersections). Anyway, very remarkably, this channel is too high in energy to provide an efficient way for radiationless decay. In fact, $\mathbf{CI_b}$ has only two unpaired electrons centered on single carbon atoms, plus two resonance stabilized allyl radicals. Consequently, different ground-state relaxation channels depart from this point and are favored. In particular, we have shown how photoinduced formation of semibullvalene (the primary photoproduct) and double-bond shifting are boosted by **COT*** deactivation through this novel conical intersection point, which in fact represents the locus for the ground-state branching of the photochemical process.

Scheme 10

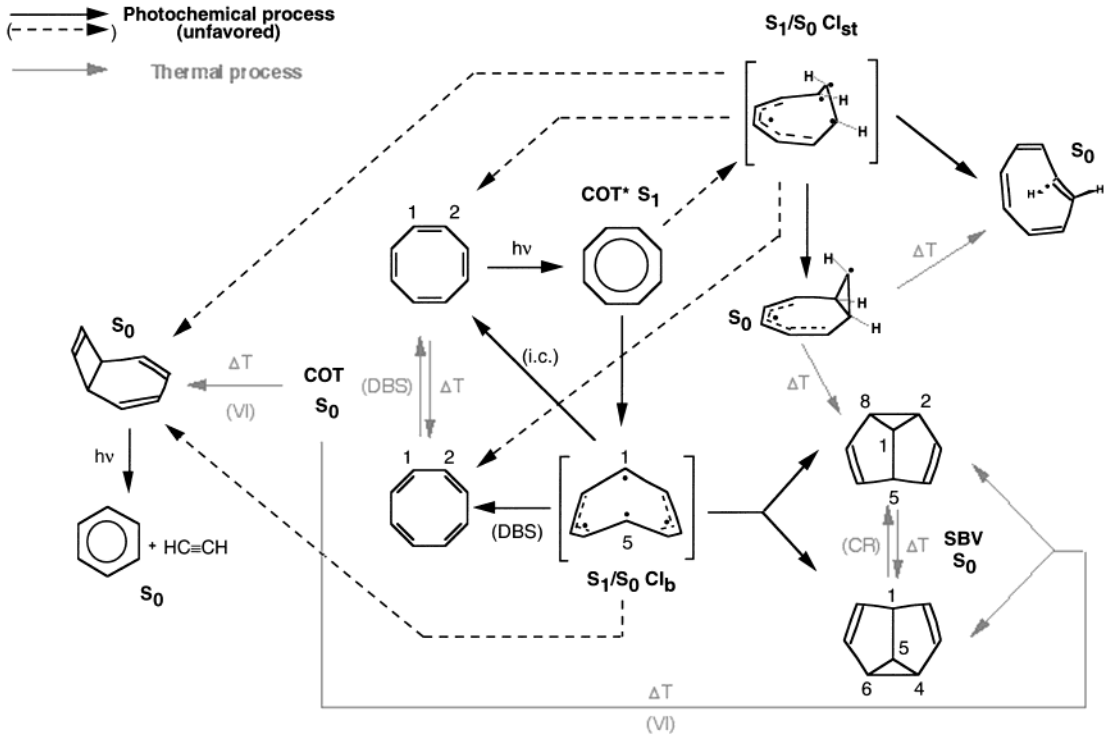

Scheme 11

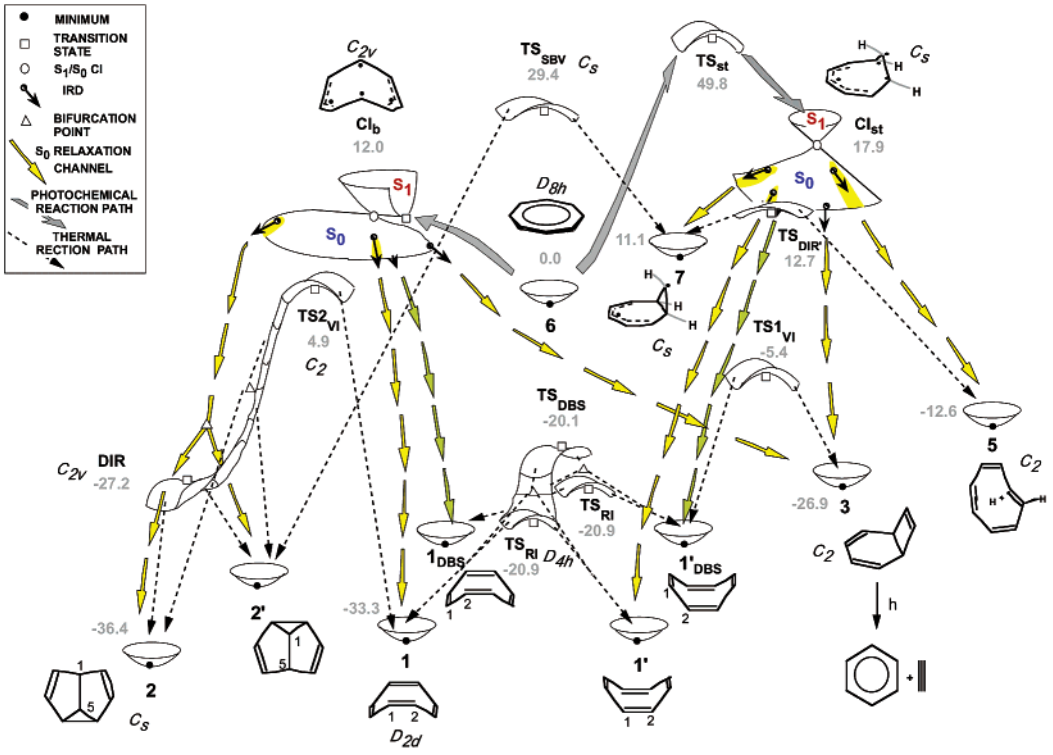

We argue that this result provides not only a conclusive mechanistic explanation for the experimentally observed[2] cyclooctatetraene → semibullvalene photoisomerization in the gas phase (eq a), thus correcting previously proposed mechanistic hypothesis,[1] but also rationalizes photochemical double-bond shifting. In fact, both processes emerge from the same conical intersection point (**CI_b**), which thus provides the rationale for cyclooctatetraene photochemistry, interconnecting excited-state channels versus ground-state relaxation paths. The main "chemical" result reported above is that production of semibullvalene and double-bond shifting are intrinsically bounded processes. While for the condition of low vibrational excess energy (for instance, in solution or in a cold matrix where the excess vibrational energy is rapidly removed), or for polysubstituted cyclooctatetraenes, the double-bond shifting process should dominate, we expect semibullvalene formation to be competitive in the presence of a vibrationally excited reactant. This feature should be properly considered when designing double-bond

shift-based molecular switches or other types of double-bond shift-based molecular devices.

Thermal processes (i.e., thermal conversions between cyclooctatetraene photoproducts, and reactions such as valence isomerization, Cope rearrangement, double-bond shifting, ring inversion) have also been investigated to draw a comprehensive reactivity scheme, which rationalizes observations and embraces the complex network of photochemical (S_1) versus thermal (S_0) reaction channels and their interconnections. A summary of the full reaction network is shown in Scheme 10, while a cartoon-like drawing is shown in Scheme 11, which also reports the relative (to **COT***) PT2-corrected energies for all of the key structures discussed in the paper.

Acknowledgment. This work was supported by Grants BQU2000-0646 and BQU2001-2926 of the Spanish D.G.E.S. Funds have been partly provided by the Università di Siena (Progetto di Ateneo A.A. 00/02), HFSP (RG 0229/2000-M), and the Università di Bologna (Funds for selected research topics). CINECA (Italy) is gratefully acknowledged (Grant k1ibozz1).

Supporting Information Available: Experimental data (PDF). This material is available free of charge via the Internet at http://pubs.acs.org.

JA020741V